Geological Quarterly, 2011, **55** (4): 301–322

Isotopic ages of selected magmatic rocks from King George Island (West Antarctica) controlled by magnetostratigraphy

Jerzy NAWROCKI, Magdalena PAŃCZYK and Ian S. WILLIAMS

Nawrocki J., Pańczyk M. and Williams I. S (2011) – Isotopic ages of selected magmatic rocks from King George Island (West Antarctica) controlled by magnetostratigraphy. Geol. Quart., **55** (4): 301–322. Warszawa.

Isotopic and palaeomagnetic studies were carried out in the central part of King George Island. Selected mafic to intermediate igneous rocks were sampled for this purpose. Single-grain U-Pb dating of zircons from basalts to dacites was controlled by a whole rock ^{40}Ar-^{39}Ar data and the magnetostratigraphy. Five magmatic activity phases were distinguished in the SE coast of King George Island. The oldest, late Cretaceous (Campanian) phase represented by basalts of the Uchatka Point Formation are followed by the early to middle Eocene (~53–43 Ma) phase documented by the lava flows whose ages decrease from SW to NE. Next younger magmatic activity phases were recorded by the lava flows or vertical intrusions emplaced in the late Eocene (~ 37–35 Ma), late Oligocene (~28–25 Ma) and late Pliocene to Holocene. The early to middle Eocene magmatic activity phase was the most extensive, producing the largest volume of magma in the study area. The new age determinations allow a more precise and credible stratigraphic correlation of the interbeds of sedimentary rocks observed in some places within the magmatic succession. The glacial provenance of the Hervé Cove diamictite is not obvious. It might represent a mountain river environment. Intense volcanic activity could be additional factor modelling the climate conditions of Antarctica in Paleogene.

Magdalena Pańczyk and Jerzy Nawrocki, Polish Geological Institute – National Research Institute, Rakowiecka 4, PL-00-975 Warszawa, Poland; Department of Antarctic Biology, Polish Academy of Sciences, Ustrzycka 10/12, Pl-02-141 Warszawa, Poland; e-mails: magdalena.panczyk@pgi.gov.pl, jerzy.nawrocki@pgi.gov.pl; Ian S. Williams, Research School of Earth Sciences, Building 61 ANU College of Physical Sciences, The Australian National University Canberra ACT 0200 Australia, e-mail: Ian.Williams@anu.edu.au (received: July 4, 2011; accepted: November 27, 2011).

Key words: Antarctica, King George Island, magnetostratigraphy, isotopic ages.

INTRODUCTION

King George Island lies in the middle of the South Shetland Archipelago (Fig. 1A), at the southern margin of the South Scotia Ridge. It is subdivided into four major tectonostratigraphic units: the axial Barton Horst, the northern Fildes Block, the southern Warszawa Block and the southernmost Kraków Block (Fig. 1B). The Cenozoic strata on King George Island, mostly basaltic and andesitic rocks with terrestrial sedimentary intercalations and intruded by dykes and plugs (Birkenmajer, 2003), contain sediments reflecting glacial and interglacial events that affected the South Shetland Islands and Antarctic Peninsula (Birkenmajer, 2001; Troedson and Smellie, 2002; Troedson and Riding, 2002).

Although crucial for palaeoclimatic and palaeotectonic reconstructions, the ages of igneous rocks from King George Island are still not sufficiently constrained. Many of the volcanic rocks and some hypabyssal intrusions from the island have been dated using whole-rock K-Ar and, more recently, ^{40}Ar-^{39}Ar methods (e.g., Birkenmajer *et al.*, 1983*a*, *b*, 1986, 2005; Smellie *et al.*, 1984, 1998; Willan and Armstrong, 2002; Kraus, 2005; Kraus *et al.*, 2007). The first reconnaissance applications of a combination of the SHRIMP method for single-grain U-Pb dating of zircon and ^{40}Ar-^{39}Ar age estimation (Fig. 1C) have indicated that this methodology might be effective and accurate (Pańczyk *et al.*, 2009; Nawrocki *et al.*, 2010). The obtained new isotopic ages substantially refine the existing stratigraphic chart of King George Island. Single-grain U-Pb dating of zircon separated from the basaltic to dacite stratified rocks of the central part of King George Island has given Eocene ages (53.0 ±0.7 to 47.8 ±0.5 Ma). In one locality, they have been supported by the results of whole rock ^{40}Ar-^{39}Ar age measurements on an andesite sample from the Demay Point Formation (*op. cit.*), previously considered (Birkenmajer, 2001) to be of Late Cretaceous age. The Late Cretaceous whole rock ^{40}Ar-^{39}Ar age was defined for the basal basalts of the Uchatka Point Formation only (Nawrocki *et al.*, 2010).

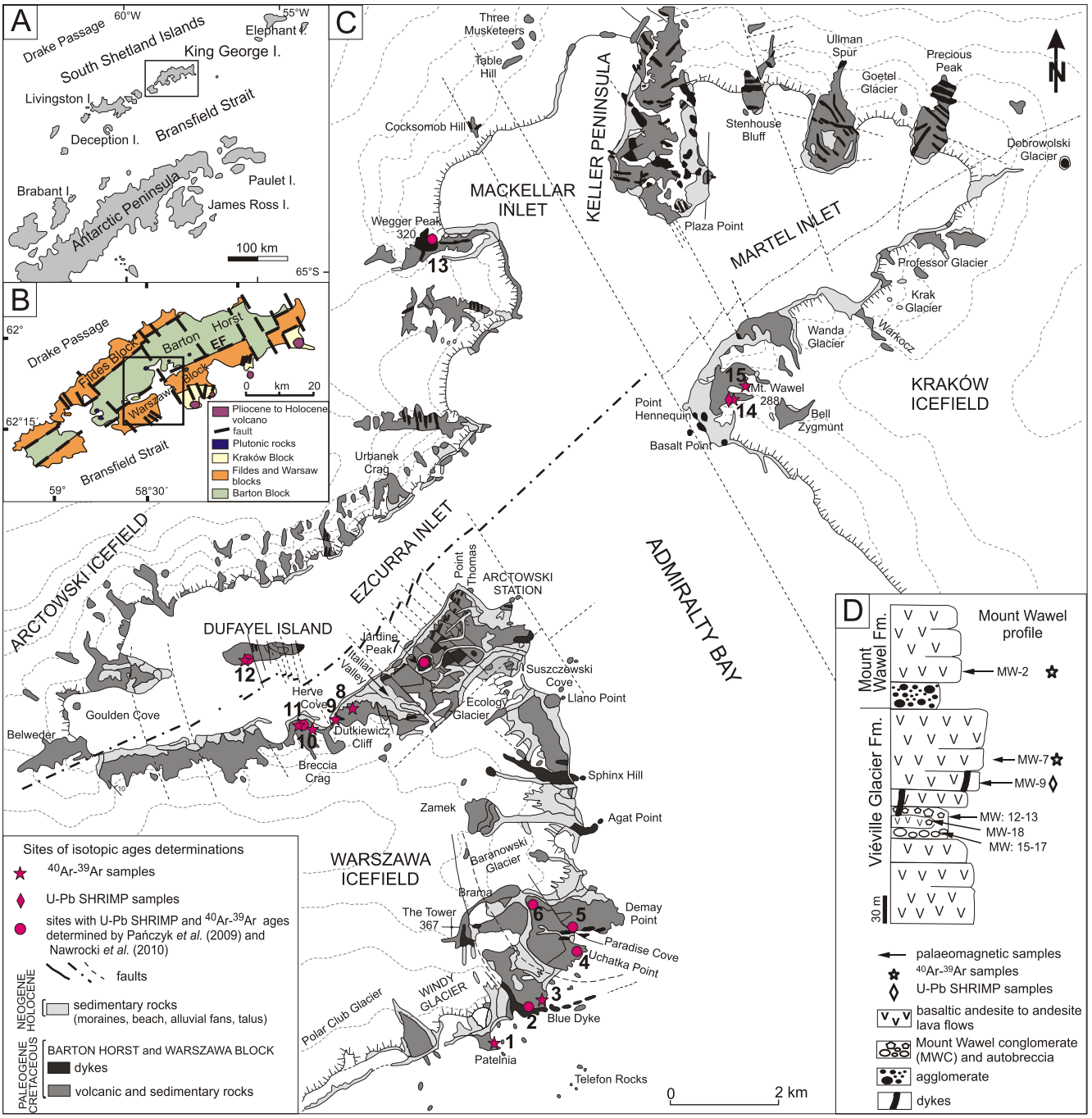

Fig. 1A – location of the studied area on King George Island, South Shetland Islands, northern Antarctic Peninsula; B – structural units of King George Island (after Birkenmajer, 2003); C – sites of isotopic studies on the background of a geological map of King George Island (after Birkenmajer, 2003, simplified); D – synthetic profile of Mount Wawel section with sampling sites marked

A: EF – Ezcurra Fault; **C**: 1 – Llano Point Formation at Patelnia Peninsula: 50.8 ±1.2 Ma (^{40}Ar-^{39}Ar), 2 – Blue Dyke hypabyssal intrusion: 25.4 ±0.4 Ma (U-Pb), 3 – Llano Point Formation near the Blue Dyke: 52.3 ±0.5 Ma (^{40}Ar-^{39}Ar), 4 – Uchatka Point Formation: 75.4 ±0.9 Ma (^{40}Ar-^{39}Ar), 5 – Demay Point Formation near the Paradise Cove: 52.6 ±0.8 Ma (U-Pb), 6 – Demay Point Formation near the Brama: 53 ±0.7 Ma (U-Pb), 52.7 ±0.6 Ma (^{40}Ar-^{39}Ar), 7 – Jardine Peak hypabbysal intrusion: 27.9 ±0.3 Ma (U-Pb), 8 – Point Thomas Fomation (Italian Valley Member): 44.1 ±1.3 Ma (^{40}Ar-^{39}Ar), 9 – Point Thomas Formation (Italian Valley Member, *ca.* 50 m above point 8): 44.6 ±0.4 Ma (^{40}Ar-^{39}Ar), 10 – Point Thomas Formation (Hervé Cove Member, below the diamictite): 47.6 ±0.4 Ma (^{40}Ar-^{39}Ar), 11 – Point Thomas Formation (Hervé Cove Member, above the diamictite): 48.1 ±0.2 Ma (^{40}Ar-^{39}Ar), 48.9 ±0.7 Ma (U-Pb), 12 – Znosko Glacier Formation: 45.5 ±0.3 Ma (^{40}Ar-^{39}Ar), 47.8 ±0.5 Ma (U-Pb), 13 – granodiorite of the Wegger Peak intrusion: 49.1 ±0.4 Ma (U-Pb), 14 – Viéville Glacier Formation: 46.8 ±0.3 Ma (^{40}Ar-^{39}Ar), 48.7 ±0.6 Ma (U-Pb), 15 – Mount Wawel Formation: 46.0 ±0.3 Ma, 43.8 ±0.3 Ma (^{40}Ar-^{39}Ar)

The main goal of the present work is to continue refinement of the chronostratigraphy of volcanogenic rocks from the central part of King George Island using a combination of SHRIMP, ^{40}Ar-^{39}Ar and magnetostratigraphic data. Well-constrained stratigraphy of the magmatic succession should allow a more precise determination of the ages of the sedimentary rocks that occur occasionally among the lava flows.

A GENERAL STRATIGRAPHY OF THE ROCKS

Part of the Warszawa Block, exposed on the western coast of Admiralty Bay between Bransfield Strait and Ezcurra Inlet, consists of rocks considered to be of Upper Cretaceous through Eocene/Oligocene age (Birkenmajer, 2001, 2002, 2003). They are subdivided into the Paradise Cove and Baranowski Glacier groups that consist of five formations: the Uchatka Point (basalts), Creeping Slope (terrestrial deposits), Demay Point (mainly felsic volcanic rocks), Llano Point (basaltic-andesitic lavas; Fig. 2A and B) and Zamek (basaltic-andesitic and andesitic lavas) (*op. cit.*). The new U-Pb and whole rock ^{40}Ar-^{39}Ar isotopic ages measured on the rocks of the Paradise Cove Group (Nawrocki *et al.*, 2010) indicate that this stratigraphic unit should be limited to Uchatka Point and most probably to the Creeping Slope Formation only (Fig. 3). The Demay Point Formation yielded an early Eocene age (50.8–53.7 Ma). The Ezcurra Inlet Group exposed along the NW coast of Ezcurra fiord (Fig. 2C) seems to be slightly younger. Single-grain zircon U-Pb dating of the lava flow from its top part (Point Thomas Formation) gave a mean age of 48.9 ±0.7 Ma (*op. cit.*).

Exposures of the Warszawa Block occur also between Point Hennequin and Dobrowolski Glacier, along the southern coast of Martel Inlet (Fig. 1C and D). Andesite lavas, layered pyroclastics, vent breccias, plugs, and plant-bearing volcanoclastic deposits are classified here as the Point Hennequin Group subdivided into the Viéville Glacier and the Mount Wawel formations (see Birkenmajer, 2003). K-Ar dates suggest a middle Eocene age for the Viéville Glacier Formation (Birkenmajer, 1989). A late Oligocene (Chattian) age for the Mount Wawel Formation was indicated also by a set of K-Ar estimations (*op. cit.*).

The most proximal part of the Barton Horst in the study area forms Dufayel Island located in the middle part of the Ezcurra Inlet (Fig. 1C and D). Magmatic rocks of the Dufayel Island are correlated with the Znosko Glacier Formation (Birkenmajer, 2001). Zircon grains extracted from andesite lava on the southern slope of Dufayel Island gave a mean age of 47.8 ±0.5 Ma (Nawrocki *et al.*, 2010). They are partly dissolved and therefore an age link between their crystallisation and magma emplacement is not so obvious. Nevertheless, it can be stated definitely that the rocks attributed in this area to the Znosko Glacier Formation cannot be older than middle Eocene.

RESEARCH MATERIAL

Two samples Pt-2 and BD-13 were taken for ^{40}Ar-^{39}Ar isotopic studies from the Llano Point Formation at Patelnia Peninsula and in the vicinity of the Blue Dyke (Fig. 2A and B). Another four samples (PL-7, PL-16, PH-1 and PH-3) were collected for this purpose from the rocks of the Point Thomas Formation at Hervé Cove (Fig. 2C). One of them (PH-3) was taken from the lava flow overlying the Hervé Cove diamictite (Fig. 2E), dated earlier by the U-Pb SHRIMP method (Nawrocki *et al.*, 2010). One sample specified here as DL-10 was taken from the same piece of rock of the Znosko Glacier Formation at Dufayel Island (Fig. 2D), that was used for the aim of single grain U-Pb dating of zircon. The results of this age estimation and magnetic polarity determinations in all the samples were presented in our earlier paper (*op. cit.*). Two samples MW-2 and MW-7 for ^{40}Ar-^{39}Ar isotopic studies and one sample MW-9 for single grain U-Pb dating of zircon were collected from the lava flows of the Mount Wawel section that consists of the Viéville Glacier and Mount Wawel formations. These samples and five clasts of conglomerate and autobreccia, found in the middle part of the Viéville Glacier Formation (Figs. 1D and 2F), were also examined for magnetostratigraphy.

The Llano Point Formation near the Blue Dyke and at Patelnia Peninsula (Figs. 1C and 2A, B) comprises massive, dark grey lava flows. The basaltic rocks contain plagioclase and clinopyroxene phenocrysts (Fig. 4B), whereas the groundmass consists of plagioclase, clinopyroxene and rare titanomagnetite and apatite crystals. The plagioclase crystals occur as euhedral and subhedral phenocrysts showing zonation, which sporadically form glomerocrysts, and as tiny, less than 0.5 mm in length, irregularly and randomly oriented laths in the groundmass. All of them show chemical zoning. The core and the rims of the plagioclase crystals yielded the bytownite and labradorite compositions, respectively. The lava flows from the Blue Dyke area are much more altered than the lavas from Patelnia Peninsula. It could be explained by hydrothermal activity related to the Blue Dyke intrusion. The volcanic sequence from Hervé Cove (southern coast of Ezcurra Inlet, Point Thomas Formation) comprises lava flows from 2 to 20 m thickness, volcaniclastic layers (pyroclastic rocks and lahar deposits) and diamictite within the upper part of the section. Generally, the volcanic rocks from Hervé Cove are crystal-rich, porphyritic, dark grey, grayish-green or red rocks, commonly altered. The lava flows are characterized by porphyritic, usually glomeroporphyritic, intersertal or intergranular texture within the lower part of the section and by porphyritic, glomeroporphyritic, massive, aphanitic texture above the diamictite. Locally, vesicular texture is noticeable. Irregular in shape, rarely slightly elongated vesicles are filled by hydrothermal minerals such as quartz, albite, zeolites and phyllosilicates. The lava flows are characterized by a very similar mineral paragenesis in a different proportion. The content, size, shape and distribution of phenocrysts are variable and specific for each lava flow. Typically, volcanic rocks comprise plagioclase

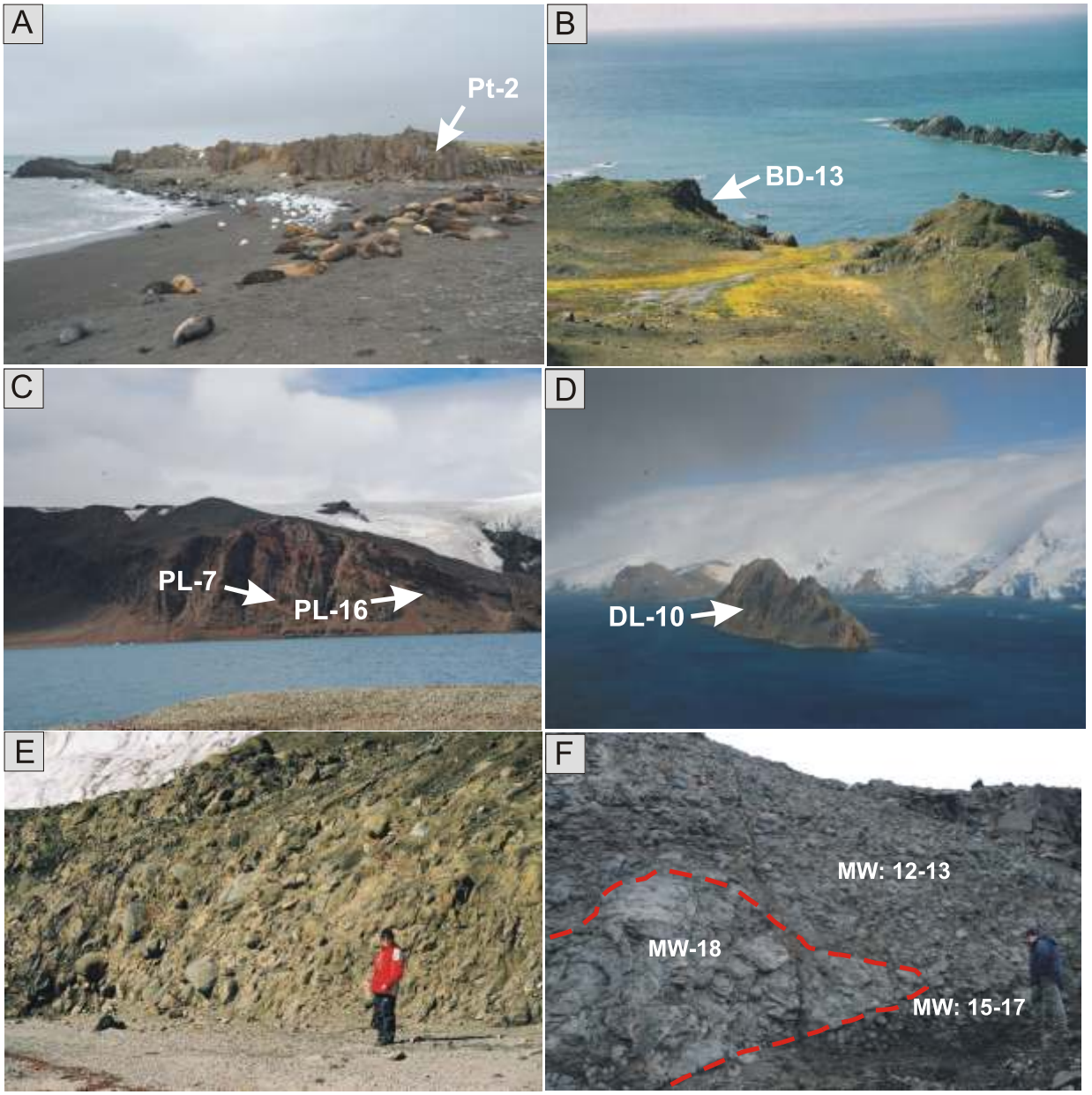

Fig. 2. Photo images of sampling sites

A – Llano Point Formation on the Patelnia Peninsula; **B** – Llano Point Formation near to the Blue Dyke; **C** – bottom part of the Point Thomas Formation in the Ezcurra Inlet; **D** – Dufayel Island in the Ezcurra Inlet; **E –** diamictite from the Hervé Cove; **F** – Mount Wawel conglomerate (samples MW: 15-17), autobreccia (samples MW: 12-13) and lava flow (MW-18)

and clinopyroxene as phenocrysts (Fig. 4C and D), whereas the groundmass contains plagioclase, clinopyroxene, titanomagnetite, magnetite, and rare copper and cuprite as well as apatite crystals found as inclusions within the magnetic minerals. Almost all of the plagioclase crystals show chemical zoning. The core and the rims of the plagioclase crystals are usually of bytownite and labradorite composition, respectively. The clinopyroxene phenocrysts (augite) contain titanomagnetite inclusions. Lava flows from Dufayel Island (Znosko Glacier Formation) are green basaltic rocks with micro veins containing hydrothermal minerals. The volcanic rocks are characterized by porphyritic, amygdoidal texture and comprise clinopyroxene and strongly altered plagioclase phenocrysts of labradorite composition. The vesicles are usually filled by hydrothermal minerals such as albite, quartz and chlorite. The groundmass (Fig. 4A) as well as phenocrysts are strongly altered (carbonatisation and chloritisation) and contain relics of plagioclase, clinopyroxene and titanomagnetite. Several dark grey lava flows of Mount Wawel (Viéville Glacier Formation and Mount Wawel Formation) are massive, excluding lavas

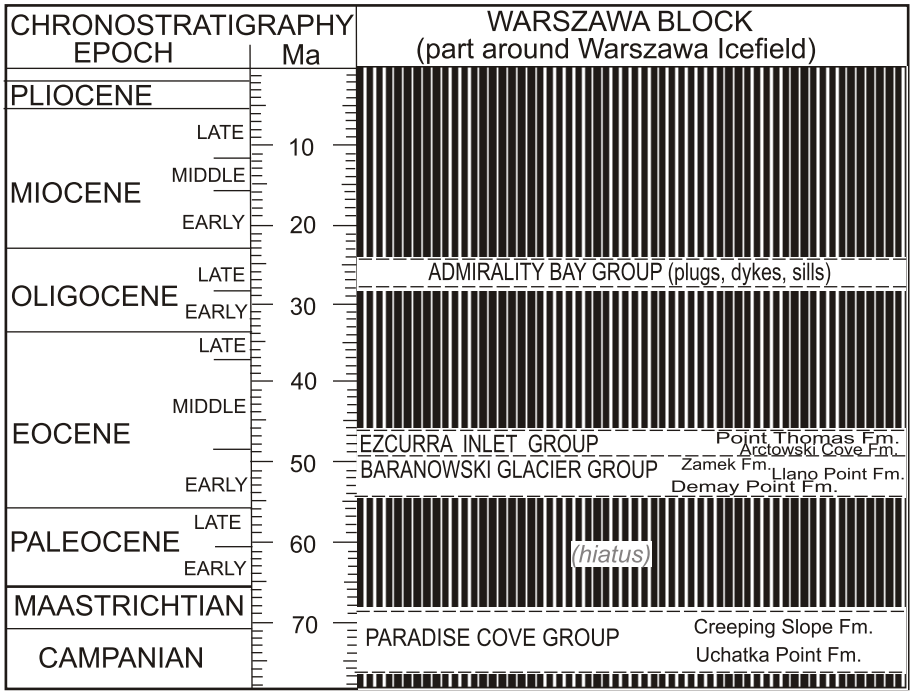

Fig. 3. Warszawa Block lithostratigraphy according to Birkenmajer (2002, 2003) set in the chronostratigraphy after Nawrocki *et al.* (2010)

Global geochronological frames were adopted from Gradstein *et al.* (2004)

from the middle part of the section. The andesites are characterized by porphyritic, commonly glomeroporphyritic, intersertal or intergranular texture within the lower and middle part of the section and massive, porphyritic, glomeroporphyritic, aphanitic texure above the agglomerate *sensu* Birkenmajer (1981). Typically, the lava flows comprise plagioclase, clinopyroxene (Ti-augite) and orthopyroxene (hyperstene) as phenocrysts, whereas the groundmass contains plagioclase, clinopyroxene, orthopyroxene, titanomagnetite, magnetite, opaque minerals and apatite and zircon crystals found as inclusions within the magnetic minerals. Conglomerate found in the middle part of the Mount Wawel section (Fig. 1D) comprises clasts of andesitic lavas. The clasts are characterized by porphyritic, intergranular, amygdaloidal texture, whereas the vesicles are infield by chlorite. The phenocrysts of plagioclase, clinopyroxene and orthopyroxene as well as groundmass is strongly altered. The first lava flow above the Mount Wawel conglomerate is characterized by amygdaloidal textures. The irregularly shaped, sometimes slightly elongated vesicles are rimmed by chlorite and infilled by zeolites, which were identified as chabazites (Table 1; Figs. 5 and 6).

These sequences of volcanic rocks contain between 45–65 wt.% of SiO_2. On the TAS classification diagram (Le Maitre *et al.*, 1989), the rocks are mainly basalts, basaltic andesite and andesite with some trachybasalts, basaltic trachyandesite and trachydacite. The oldest lava flows from Paradise Cove (Uchatka Point Formation; Nawrocki *et al.*, 2010) and the lavas from the Blue Dyke area as well as from Patelnia Peninsula (Llano Point Formation) fall within the basaltic and basaltic andesite field (Fig. 7A). The lavas of Demay Point Formation plot in trachyandacite field. Samples from the Hervé Cove section (Point Thomas Formation) are much varied and plot in four separate fields. The lava flows from the lower part of the Hervé Cove section fall within the basaltic field. However, some lava flows from the middle and upper part of the Hervé section, commonly up to 3–4 m thickness, are enriched in alkalis due to post-magmatic alteration, and plot in the trachybasalt and basaltic trachyandesite field. The uppermost lava flow of that section shows a different chemical composition and falls within the andesite field. The samples of lava flows from Mount Wawel are mainly andesites, some samples fall within the basaltic andesite and basaltic trachyandesite. The weakly altered samples from Dufayel Island fall within the basaltic trachyandesite, basaltic andesite and trachyandesite. Plotted on the classification diagram of Winchester and Floyd (1977; Fig. 7B), the composition of the lava flows from Paradise Cove, Blue Dyke area and Patelnia Peninsula as well as from the lower and middle part of the Hervé section fall within the basalt field. The samples from Mount Wawel, the upper part of the Hervé section and Dufayel Island fall within the andesite field. The lava flows of Demay Point correspond to the rhyodacite/dacite field.

RESEARCH METHODS

ISOTOPIC STUDIES

All the whole-rock samples taken for ^{40}Ar-^{39}Ar geochronology were crushed by hand or with a jaw-crusher and subsequently milled using a swing-mill. They were cleaned and pro-

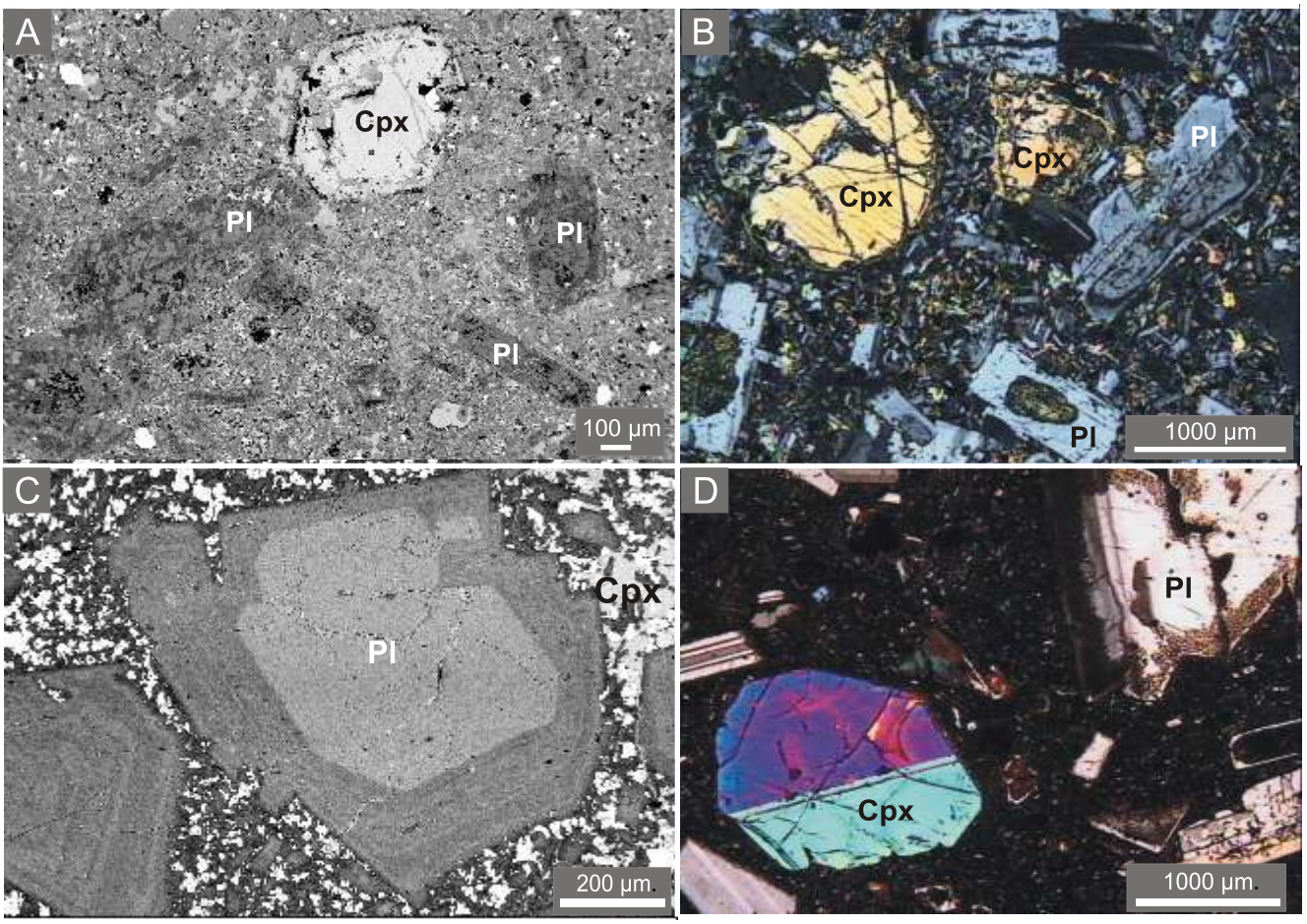

Fig. 4. Photomicrographs of samples analysed

A – lava flow from Dufayel Island: phenocrysts of clinopyroxene and altered plagioclase within intensive overprinted groundmass (BSE – back-scattered electron image); **B** – lava flow from Blue Dyke area: phenocrysts of clinopyroxene and plagioclase (crossed polars); **C** – lava flow from lower part of Breccia Crag, Hervé Cove: phenocryst of zoned plagioclase within the intergranular groundmass (BSE image); **D** – lava flow from upper part of Hervé profile (above diamictite): phenocrysts of plagioclase and clinopyroxene within microcrystalline groundmass (crossed polars); symbols for rock-forming minerals after Kretz (1983): Cpx – clinopyroxene, Pl – plagioclase

cessed into a range of grain-sizes and the 0.25–0.5 mm fraction was selected. ^{40}Ar-^{39}Ar geochronology was carried out at the ^{40}Ar-^{39}Ar geochronological laboratory at the University of Lund, Sweden. The samples selected for ^{40}Ar-^{39}Ar geochronology were irradiated together with the TCR sanidine standard (28.34 Ma following Renne *et al*., 1994) for 24 hours at the Oregon State research reactor. J-values were calculated with a precision of <0.25% and are reported for each sample in the data tables. The decay constants were those given in Steiger and Jäger (1977). The ^{40}Ar-^{39}Ar geochronology laboratory at the University of Lund contains a *Micromass 5400* mass spectrometer with Faraday and electron multiplier detectors. A metal extraction line, which contains two *SAES C50-ST101 Zr-Al* getters and a cold finger cooled to *ca*. –155°C by a *Polycold P100* cryogenic refrigeration unit, is also present. Whole rock separates were loaded into a copper planchette that consists of several 3 mm holes. Samples were step-heated using a defocused 50W CO_2 laser. The laser was rastered over the samples to provide even heating of all grains. The entire analytical process is automated and runs on a *Macintosh-steered OS 10.2* with software modified specifically for the laboratory at the University of Lund and developed originally at the Berkeley Geochronology Center by Al Deino. Time zero regressions were fitted to data collected from 10 scans over the mass range of 40 to 36. Peak heights and backgrounds were corrected for mass discrimination, isotopic decay and interfering nucleogenic Ca-, K- and Cl-derived isotopes. Isotopic production values for the cadmium lined position in the OSU reactor are ^{36}Ar-^{37}Ar(Ca) = 0.000264, ^{39}Ar-^{37}Ar(Ca) = 0.000695 and ^{40}Ar-^{39}Ar(K) = 0.00073. ^{40}Ar blanks were calculated before every new sample and after every three sample steps. Blank values were subtracted for all incremental steps from the sample signal. The laboratory was able to produce very good incremental gas splits, using a combination of increasing time at the same laser output, followed by increasing laser output. Age plateaus were determined using the criteria of Dalrymple and Lamphere (1971), which specify the presence of at least three contiguous incremental heating steps with statistically indistinguishable ages and constituting greater than 50% of the total ^{39}Ar released during the experiment. In some places where a statistical overlap of steps is not obtained, a forced-fit age is given over a certain percentage of gas. ^{40}Ar-^{39}Ar geo-

Table 1

Major element and anhydrous cations abundances of representative chabazite from lava flow from the Mount Wawel

Formula	SiO_2	TiO_2	Al_2O_3	MnO	MgO	FeO	CaO	Na_2O	K_2O	Total	Elevation
1/1/1.	54.85	0.00	20.78	0.03	0.57	0.56	10.63	0.23	0.55	88.20	100
1/2/1.	54.35	0.00	20.34	0.03	0.45	0.54	9.92	0.50	0.60	86.73	100
1/3/1.	54.92	0.02	20.90	0.01	0.35	0.38	10.53	0.36	0.52	87.99	100
1/5/1.	55.02	0.00	20.99	0.04	0.59	0.67	10.47	0.26	0.52	88.56	100
2/1/1.	54.30	0.01	21.32	0.02	0.48	0.55	10.98	0.18	0.51	88.35	100
2/2/1.	54.54	0.00	21.32	0.01	0.53	0.59	10.61	0.29	0.53	88.42	100
2/4/1.	53.33	0.00	21.04	0.04	2.02	2.11	9.58	0.34	0.44	88.90	100
2/5/1.	53.81	0.03	21.15	0.00	1.01	1.15	10.22	0.36	0.42	88.15	100

Formula	Si	Ti	Al	Mn	Mg	Fe	Ca	Na	K	Total	Molecular ratio Al_2O_3/(Ca, Na, K, Mg)O	(Na + K)/Ca	Al/Si
1/1/1.	10.99	0.00	4.91	0.01	0.17	0.09	2.28	0.09	0.14	18.68	0.955023364	0.100789	2.240163
1/2/1.	11.06	0.00	4.88	0.01	0.14	0.09	2.16	0.20	0.16	18.68	0.985451606	0.162275	2.266967
1/3/1.	11.01	0.00	4.94	0.00	0.11	0.06	2.26	0.14	0.13	18.65	0.985822684	0.122124	2.229086
1/5/1.	10.98	0.00	4.93	0.01	0.18	0.11	2.24	0.10	0.13	18.67	0.975093892	0.104111	2.224812
2/1/1.	10.87	0.00	5.03	0.00	0.15	0.09	2.36	0.07	0.13	18.71	0.967320261	0.08489	2.160771
2/2/1.	10.90	0.00	5.02	0.00	0.16	0.10	2.27	0.11	0.13	18.71	0.982977891	0.108667	2.170382
2/4/1.	10.69	0.00	4.97	0.01	0.60	0.35	2.06	0.13	0.11	18.93	0.892459605	0.118504	2.151277
2/5/1.	10.82	0.01	5.01	0.00	0.30	0.19	2.20	0.14	0.11	18.79	0.952670595	0.113079	2.159018

Chemical composition of the zeolites were determined using an electron microprobe *Cameca SX 100* (Polish Geological Institute – National Research Institute in Warsaw)

chronology data were produced, plotted and fitted using the argon programme provided by Al Deino from the Berkeley Geochronology Centre, USA.

Samples for zircon separation were crushed and screened after thorough examination of thin sections. Heavy mineral fractions were separated using conventional heavy liquid and magnetic techniques. Selected zircon grains were hand-picked from the concentrates and mounted in epoxy with zircon standards SL13 (U = 238 ppm) and TEMORA (^{206}Pb-^{238}U = 0.06683), sectioned by polishing, documented by transmitted and reflected light microscopy, then imaged by cathodoluminescence (CL) using a *Hitachi S-2250N SEM*. The CL images were used to characterize the size, morphology and internal texture of each grain. Following CL examination, 11 zircon grains were chosen for single-grain U-Pb dating using the SHRIMP II at the Research School of Earth Sciences, Australian National University, Canberra, and procedures based on those described by Williams and Claesson (1987). Analytical conditions were as follows: 10 kV negative O_2 primary ion beam focused to *ca*. 25 µm diameter spot; 10 kV positive secondary ions; mass resolution *ca*. 5000; isotope ratio measurement by a single electron multiplier and cyclic peak stepping. Ages were calculated using the constants recommended by the IUGS Subcommission on Geochronology (Steiger and Jäger, 1977). Uncertainties in the calculated mean ^{206}Pb-^{238}U ages are 95% confidence limits, and include the uncertainty in the Pb/U calibration (0.17–0.25%). Common Pb corrections were made using ^{207}Pb, assuming concordance and that the common Pb was laboratory derived (Broken Hill galena composition).

MAGNETOSTRATIGRAPHY

Ten hand oriented samples were collected from the Mount Wawel section. Several core specimens, 2.5 cm diameter and 2.2 cm length, were drilled from each hand sample. Finally, 36 specimens were subjected to alternating field (AF) demagnetisation experiment. The natural remnant magnetisations (NRM) were measured with a *Geofyzika JR6A* spinner magnetometer. Demagnetisation results were analysed using orthogonal vector plots (Zijderveld, 1967), and the directions of the linear segments were calculated using principal component analysis (Kirschvink, 1980). Magnetic mineralogy of lavas from the central part of King George Island was defined by Nawrocki *et al*. (2010) using blocking temperatures and coercivity spectra, and especially scanning electron microscope EDX analyses and BSE imaging. Magnetite or titanomagnetite of different grain-sizes were defined as common in these rocks.

RESULTS

WHOLE-ROCK ^{40}Ar-^{39}Ar ISOTOPE DATING

Basaltic whole-rock samples PT-2 and BD-13 collected from the Llano Point Formation gave well-defined Ar-Ar plateau ages of 50.8 ±1.2 Ma and 52.3 ±0.5 Ma, respectively (Fig. 8 and Appendix), with medium MSWDs (1.31 and 2.26) and medium to low (sample BD-13) probabilities of χ^2distri-

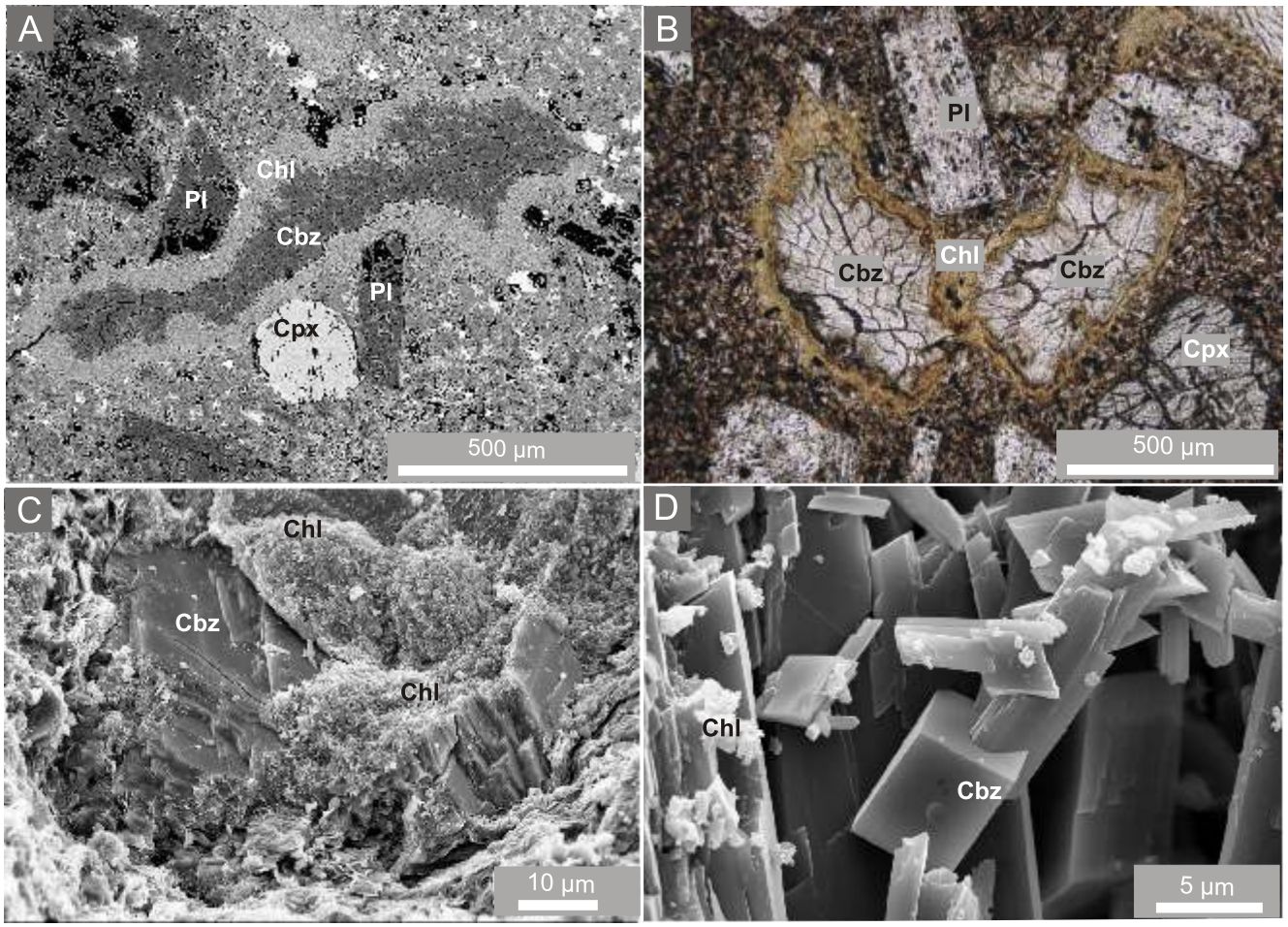

Fig. 5. Photomicrographs of the first lava flow above the Mount Wawel Conglomerate

A – typical vesicle rimmed with chlorite and filled with chabazite (BSE image); **B** – vesicles filled with chabazite and rimmed by smectite (PN – parallel polars); **C** – chabazite rimmed by chlorite (SE – second electron image); **D** – crystals of chabazite (SE image); symbols for rock-forming minerals after Kretz (1983): Cbz – chabazite, Chl – chlorite, Cpx – clinopyroxene, Pl – plagioclase

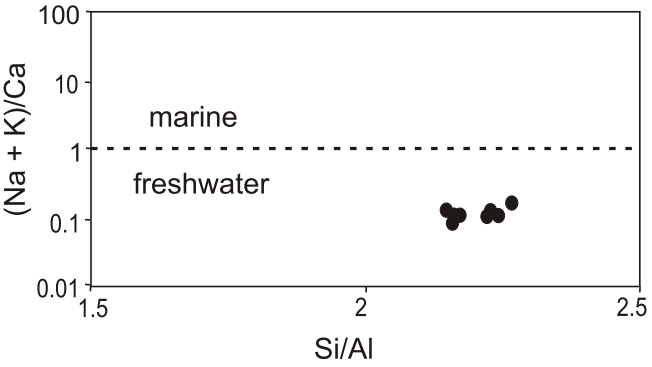

Fig. 6. Microprobe analyses of chabazite from first lava flow above the Mount Wawel conglomerate (MWC) performed using *Cameca SX 100* instrument in Polish Geological Institute National – Research Institute in Warsaw

Diagram of Si/Al ratio *versus* (Na + K)/Ca for chabazites from Mount Wawel lava flow. The horizontal, discriminant line separating "fields" of marine alteration [(Na + K)/Ca >1.0) from freshwater alteration [(Na + K)/Ca <1.0) are from Johnson and Smellie (2007). The chabazite composition from the Mount Wawel lava flow suggests its formation in a freshwater environment

bution. The age spectra show only a very slight but irregular decrease of apparent age from the low temperature steps toward the intermediate or high temperature steps. Basaltic subsamples PL-16 and PL-16a were taken from the same piece of lava flow attributed to the Point Thomas Formation. Their whole rock ^{40}Ar-^{39}Ar plateau ages are very similar i.e. 44.9 ±0.7 Ma and 44.6 ±0.4 Ma, respectively. A comparable plateau age of 44.1 ±1.3 Ma was also defined for sample PL-7, that was taken from the same section but about 50 m below. Clearly older whole rock plateau ages were defined for two andesitic samples PH-1 and PH-3b that were taken close to the Hervé Cove tillite. Sample PH-1 from the lava flow underlying the tillite provided a plateau age of 47.6 ±0.4 Ma. Otherwise, sample PH-3b taken from the lava flows overlying the tillite gave also a well-defined plateau age of 48.1 ±0.2 Ma. It should be stressed that this age is equal within uncertainty to the mean SHRIMP zircon age (48.9 ±0.7 Ma) measured on the same piece of lava flow (Nawrocki *et al.*, 2010). A set of plagioclase grains was also separated from this sample. They gave a plateau age of 41.5 ±0.8 Ma (Fig. 8).

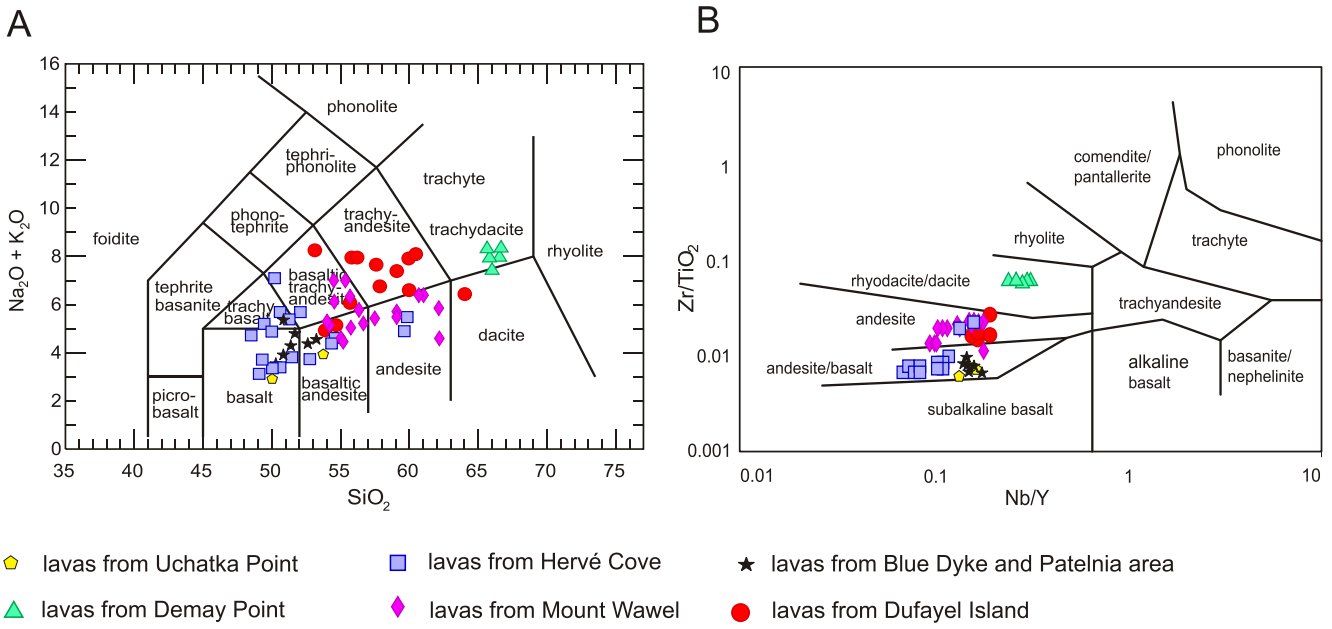

Fig. 7A – chemical classification of the volcanic rocks on total alkalis *versus* silica (TAS) diagram of Le Maitre *et al*. (1989); B – chemical classification of volcanic suite using Zr/TiO_2 *vs*. Nb/Y diagram (Winchester and Floyd, 1977)

However, its probabilities of χ^2distribution is extremely low (p = 0.01) and consequently it should be regarded as of poor credibility. The same low values of p were received for highly altered andesite subsamples DL-10 and DL-10a taken from one lava flow of the Znosko Glacier Formation at Dufayel Island. Plateau ages calculated for both the subsamples seem to be, however, even consistent (45.02 ±0.2 Ma and 45.50 ±0.3 Ma, respectively; Fig. 9) but substantially younger than the U-Pb SHRIMP zircon age (47.8 ±0.5 Ma) measured on the same piece of rock (*op. cit.*).

Very consistent plateau ages of 46.7 ±0.3 Ma and 46.8 ±0.3 Ma were defined for subsamples MW-7 and MW-7a, respectively, taken from the Viéville Glacier Formation (Fig. 1D). A similar plateau age of 46.0 ±0.3 Ma was defined for subsample MW-2 of the Mount Wawel Formation. However, the second subsample MW-2a from the same piece of andesitic rock provided a slightly younger age of 43.8 ±0.3 Ma.

SINGLE GRAIN ZIRCON U-Pb DATING

Zircon isotopic analyses of sample MW-9 are listed in Table 2 and plotted on concordia diagrams in Figure 10. The zircon had low to moderate U and Th contents (127–500 ppm and 1–17 ppm, respectively). The Th/U ratio was mostly typical of igneous zircon. The lowest values (0.29) were reported from one old (Early Ordovician) zircon grain. The rest of the zircon population had Th/U ratios between 0.46 and 1.03. The SHRIMP data are concordant within analytical uncertainty and form distinct clusters. 10 of the 11 analyses of Eocene zircon from the Viéville Glacier Formation have the same radiogenic $^{206}Pb/^{238}U$ within analytical uncertainty, giving a weighted mean age of 48.7 ±0.6 Ma. It can be stated therefore that these zircon gains are of late Ypresian to earliest Lutetian age (Gradstein *et al.*, 2004). One study of a smaller rounded grain 7.1 gave a much higher $^{206}Pb/^{238}U$ age, 497 Ma (Table 2). It had a very low Th/U ratio commonly found in metamorphic zircon from peraluminous rocks. This is probably a grain of igneous zircon derived from fine-grained sediment (e.g., sandy mudstone) a small amount of which has contaminated the Eocene magma.

MAGNETIC POLARITY OF SAMPLES FROM THE MOUNT WAWEL SECTION

All the samples collected from the Mount Wawel section were strongly magnetised. The intensity of NRM ranged from 0.45 to 1.35 A/m. The NRM was demagnetised in an alternating field of amplitude up to 100 mT. It should be stressed that more than 80% of the initial intensity of NRM was removed in a field not higher than 40 mT in samples MW-18, MW-2 and MW-7 (Fig. 11A) taken from the lava flows. Autobreccia and conglomerate samples appeared to be more resistant to the AF demagnetisation. The structure of NRM of the rocks was very simple. After removing low coercivity magnetisation in the fields not higher than 20 mT, only one distinct characteristic component with steep inclination remained in most of the samples taken from the lava flows and in all the samples from conglomerate boulders. The sample of the lava flow that covers directly the conglomerate (MW-18) and the samples taken from this conglomerate showed virtually the same direction (Fig. 11B). It indicates that the conglomerate was most probably remagnetised by the lava flow. Autobreccia samples MW-12 and MW-13 revealed the presence of dispersed char-

acteristic components with shallow inclination and different declination that does not correspond to the expected N–S direction. The same shallow positive inclination is observed in sample MW-9 taken from the lava flow. However, its declination is exactly southern. Finally, samples MW-2, MW-9, MW-15, MW-16, MW-17 and MW-18 can be regarded as containing a reversed polarity record. The normal polarity characteristic directions were defined for one hand sample MW-7 only (Fig. 11C). This sample was taken from the lava flow forming the upper part of the Viéville Glacier Formation.

DISCUSSION

DETAILED CHRONOSTRATIGRAPHY

The U-Pb and ^{40}Ar-^{39}Ar ages measured on the rocks of the Demay Point Formation (Nawrocki *et al.*, 2010) are very consistent. The magnetic polarity of the dated samples correspond in the limit of errors to the global polarity time scale – GPTS (Gradstein *et al.*, 2004) indicating that these rocks were emplaced between ~53 and ~51 Ma (Fig. 12).

Assuming that the stratigraphic succession has been correctly determined and the Demay Point Formation underlies the Llano Point Formation (Birkenmajer, 2002, 2003), the maximum age of the latter should be ~51 Ma. This interpretation is in agreement with the ^{40}Ar-^{39}Ar age of reversely magnetised sample PT-2 that well-corresponds to the lower part of the C22 magnetic polarity chron of GPTS. The second sample of the Llano Point Formation, BD-13, revealed the presence of normal polarity palaeomagnetic direction but its ^{40}Ar-^{39}Ar age does not fit to the GPTS, moreover overlapping substantially the age of the Demay Point Formation (Fig. 12). This rather low quality (MSWD = 2.26, p = 0.05) ^{40}Ar-^{39}Ar plateau age is most probably a bit older than the rock dated. The correlation with the GPTS of good quality ^{40}Ar-^{39}Ar age defined for sample PT-2 (50.8 ±1.2 Ma) and the dual magnetic polarity record defined for the Llano Point Formation indicate that the real age of these rocks is most probably included between ~52 and ~49.6 Ma.

The normal polarity palaeomagnetic directions characteristic of the Point Thomas Formation at Hervé Cove (Nawrocki *et al.*, 2010) do not correspond with the ^{40}Ar-^{39}Ar plateau ages defined for samples PL-7, PL-16, PH-1 and PH-3b. These ages fit to reversed polarity intervals of the GPTS (Fig. 12). It should be stressed, however, that the ^{40}Ar-^{39}Ar ages defined for the lava flows surrounding the diamictite at Hervé Cove (sample PH-1: 47.6 ±0.4 Ma, sample PH-3b: 48.1 ±0.2 Ma) are only slightly younger than the U-Pb SHRIMP age defined earlier for sample PH-3 (*op. cit.*) taken from the same piece of rock as sample PH-3b. This single-grain zircon U-Pb dating gave a mean age of 48.9 ±0.7 Ma. The normal polarity record of sample PH-3 can therefore be correlated with the upper part of the C22 polarity chron (49.4–48.6 Ma; Gradstein *et al.*, 2004). Such age could not be ascribed to the whole Point Thomas Formation but only to its older part at Hervé Cove. Detailed fieldwork disclosed that the Ezcurra Inlet section of the Point Thomas For-

Table 2

Summary of U-Pb SHRIMP results for zircons from sample MW-9 (Viéville Glacier Formation)

Lab.	Pb	U	Th	Th/U	^{204}Pb/^{206}Pb	±	^{207}Pb/^{206}Pb	±	^{208}Pb/^{206}Pb	±	^{208}Pb/^{232}Th	±	^{206}Pb/^{238}U	±	^{206}Pb/^{235}U	±	Apparent ages [Ma] f6(7)%	^{208}Pb/^{232}Th	±	^{206}Pb/^{238}U	±
	ppm																				
9.1	4	510	414	0.81	2.00E-05	2.00E-05	0.0517	0.0023	0.2610	0.0111	0.00246	0.00011	0.00766	0.00009	0.0545	0.0025	0.51	47.6	2.4	48.9	0.6
6.1	4	499	356	0.71	8.54E-04	4.19E-04	0.0502	0.0019	0.2433	0.0112	0.00260	0.00012	0.00763	0.00008	0.0528	0.0022	0.35	50.8	2.7	48.8	0.5
4.1	4	482	380	0.79	2.40E-04	1.59E-04	0.0466	0.0020	0.2453	0.0080	0.00235	0.00009	0.00756	0.00012	0.0486	0.0023	–0.05	47.7	2.0	48.6	0.7
10.1	4	459	389	0.85	4.91E-05	3.25E-05	0.0487	0.0031	0.2916	0.0087	0.00267	0.00009	0.00775	0.00009	0.0520	0.0035	0.18	53.1	2.3	49.7	0.6
3.1	4	418	391	0.93	2.00E-05	2.00E-05	0.0480	0.0021	0.2954	0.0088	0.00238	0.00008	0.00754	0.00011	0.0499	0.0023	0.11	47.7	1.8	48.4	0.7
8.1	3	310	178	0.57	1.16E-03	4.58E-04	0.0534	0.0026	0.2005	0.0086	0.00266	0.00013	0.00762	0.00013	0.0561	0.0030	0.69	49.5	3.0	48.6	0.9
1.1	2	277	286	1.03	3.94E-04	2.08E-04	0.0515	0.0037	0.3256	0.0125	0.00235	0.00010	0.00744	0.00011	0.0528	0.0040	0.48	45.9	2.4	47.6	0.7
5.1	2	277	148	0.53	2.00E-05	2.00E-05	0.0536	0.0043	0.1789	0.0128	0.00252	0.00019	0.00755	0.00012	0.0557	0.0047	0.72	46.4	4.8	48.1	0.8
2.1	1	153	70	0.46	1.88E-03	7.63E-04	0.0505	0.0035	0.1603	0.0132	0.00267	0.00023	0.00765	0.00022	0.0532	0.0042	0.38	51.1	5.5	49.0	1.4
11.1	1	127	68	0.53	2.67E-03	1.22E-03	0.0501	0.0042	0.1673	0.0131	0.00236	0.00019	0.00752	0.00016	0.0520	0.0046	0.34	45.4	4.8	48.2	1.1
7.1	17	221	65	0.29	1.82E-04	8.70E-05	0.0587	0.0013	0.0876	0.0020	0.02398	0.00062	0.08029	0.00077	0.6494	0.0159	0.17	458	21	497.0	4.6

* – corrected for common Pb using ^{207}Pb/^{206}Pb, assuming the common Pb to be laboratory-derived surfice contaminants 204/206 = 0.0625, 207/206 = 0.9618. 208/206 = 2.229; f6(7)% – percentage of total ^{206}Pb that is common ^{206}Pb, estimated from the measured ^{207}Pb/^{206}Pb by assuming concordance; analytical uncertainties 1σ precision estimates

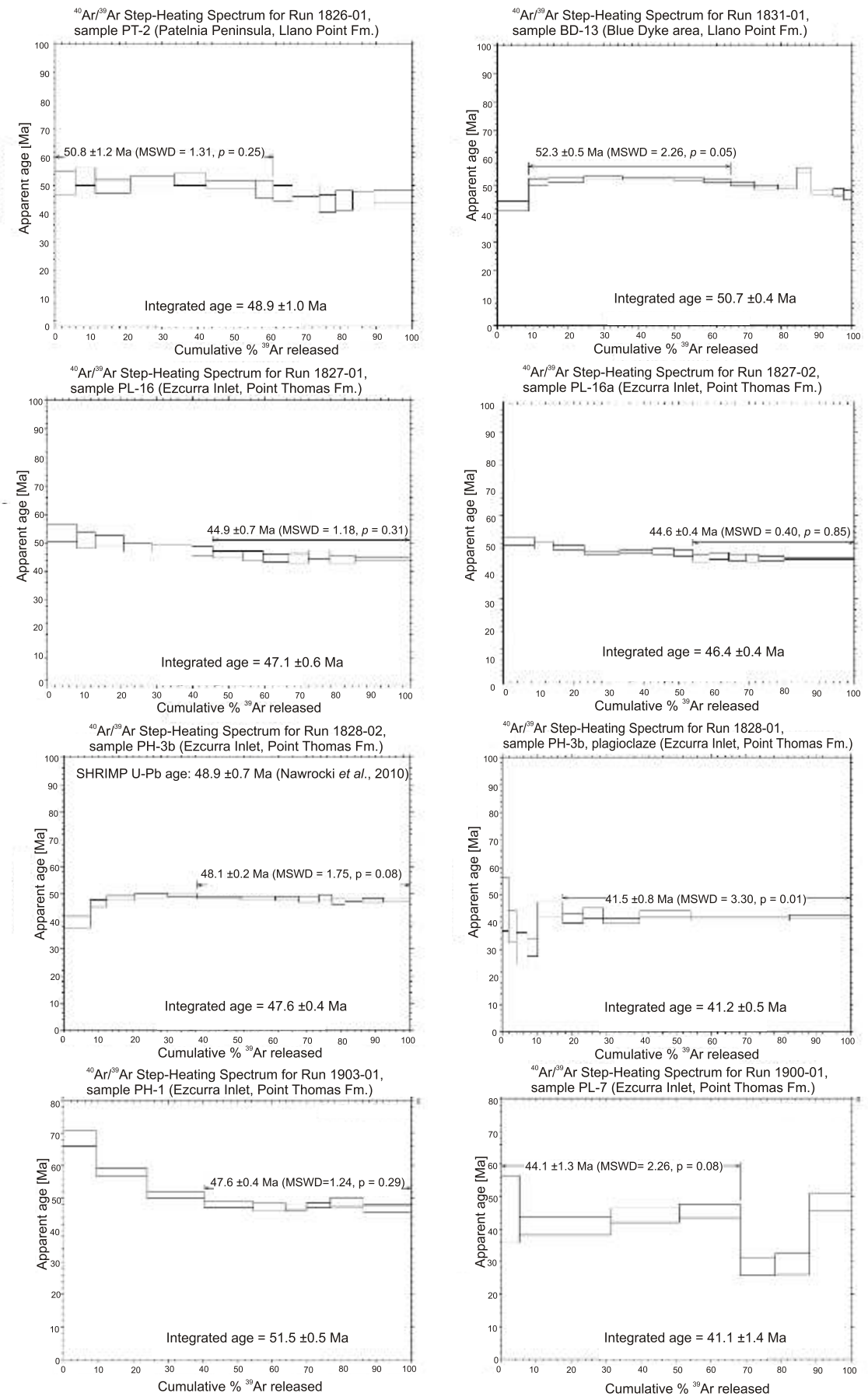

Fig. 8. ^{40}Ar-^{39}Ar age spectra from basalts of the Llano Point Formation and basaltic to andesitic rocks of the Point Thomas Formation

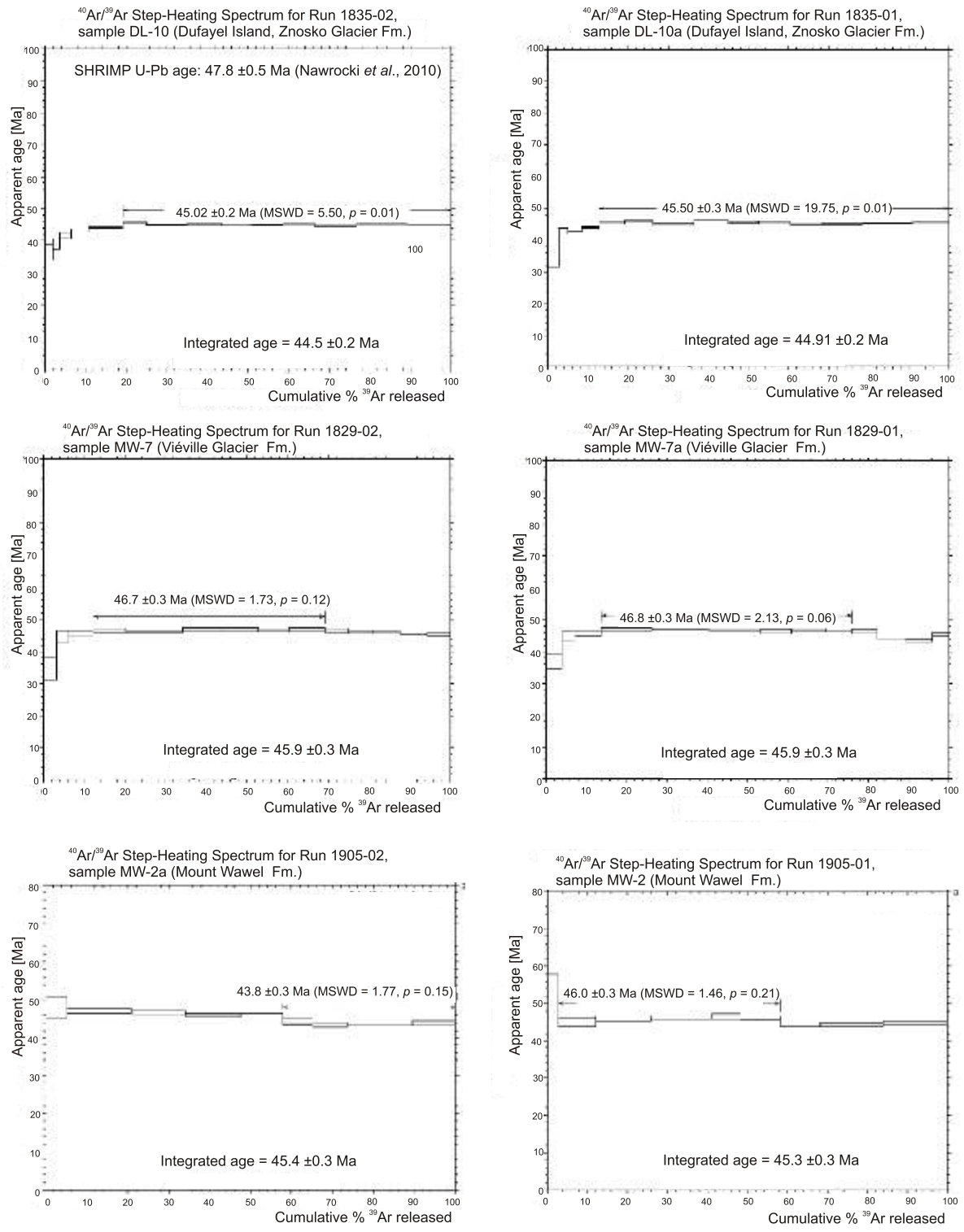

Fig. 9. ^{40}Ar-^{39}Ar age spectra from rocks of the Znosko Glacier, Viéville Glacier and Mount Wawel Formations

mation consists of two different parts, separated by a fault, at present partly covered by the ice sheet. Our isotopic ages suggest that the lava flows and pyroclastic rocks exposed between the Italian Valley and Hervé Cove probably form an independent younger unit. Its normal magnetic polarity (Nawrocki *et al.*, 2010) could be correlated with the upper part of the C21 polarity chron (47.2–45.4 Ma) if we assume that the ^{40}Ar-^{39}Ar plateau ages defined for samples PL-7 and Pl-16 are only slightly (~1.5 Ma) younger than the rocks dated. According to our new data and due to lithological differences we suggest that the Point Thomas Formation should be subdivided into two members. First unit can be named the

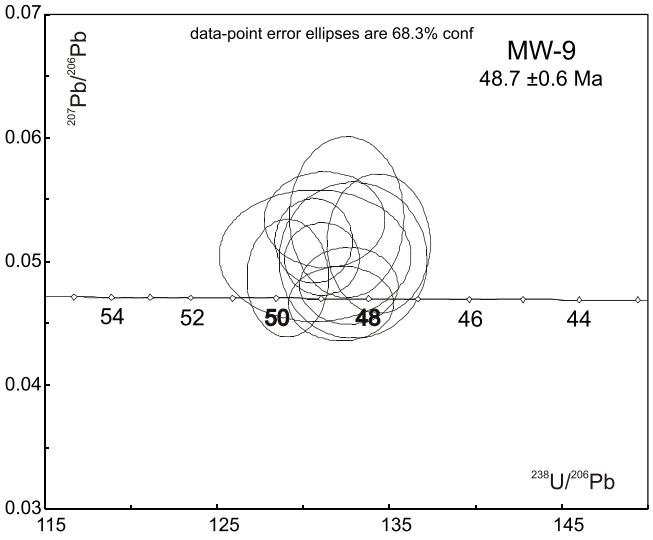

Fig. 10. Concordia plots of zircon analyses from the basaltic andesite of the Viéville Glacier Formation (Mount Wawel section, sample MW-9)

Uncertainties are 2σ

Italian Valley Member. It can be limited to the younger part of the Ezcurra Inlet volcanogenic succession that crops out between Point Thomas and Dera Icefall. For the more andesitic lava flows containing the diamictite at Hervé Cove we propose another name – the Hervé Cove Member (Fig. 12).

Referring to the stratigraphic succession of the Warszawa Block determined by Birkenmajer (2002, 2003) we can conclude that there were no long time for the deposition of the Arctowski Cove and Zamek formations (Fig. 2B), not studied herein. The Zamek Formation was most probably emplaced in a relatively narrow time interval of *ca*. 50 Ma ago or it partly overlaps in time the neighbouring formations. The stratigraphic position of the Arctowski Cove Formation in the light of new interpretation of the Point Thomas Formation presented above is probably different from previously assumed (for comparison see fig. 2 in Nawrocki *et al.*, 2010).

Samples MW-7 and MW-9 of the Viéville Glacier Formation revealed the presence of normal and reversed polarity records, respectively. The U-Pb and ^{40}Ar-^{39}Ar ages measured on these rocks allow correlating this part of the Mount Wawel section with the C21 polarity chron (48.6–45.5 Ma). The reversed polarity of sample MW-2 and the ^{40}Ar-^{39}Ar plateau ages defined for subsamples MW-2a and MW-2b indicate that this part of the Mount Wawel Formation corresponds to the reversed magnetozone of the C20 polarity chron (45.5–42.8 Ma). We can conclude therefore that both units forming the Mount Wawel section were emplaced between ~48.6 and ~42.8 Ma. It should be stressed, however, that because of lack of isotope age determinations from the topmost part of the Mont Wawel Formation their upper age limit may be even slightly younger than proposed 42.8 Ma.

Poor quality ^{40}Ar-^{39}Ar ages measured on subsamples DL-10a and DL-10b from the Znosko Glacier Formation do not differ significantly from the U-Pb SHRIMP age defined earlier for the same piece of rock (*op. cit.*). These isotope ages and the normal magnetic polarity record defined for it indicate that this part of the Znosko Glacier Formation can be correlated with the normal polarity zone of the C21 polarity chron (47.2–45.5 Ma).

MAGMATIC ACTIVITY PHASES IN SE KING GEORGE ISLAND

The new U-Pb and ^{40}Ar-^{39}Ar ages estimated for the magmatic rocks composing the SE part of King George Island and constrained by magnetostratigraphy allow us to distinguish at least five magmatic activity phases (MAP; Fig. 12A). The oldest, Campanian MAP, is represented by basalts of the Uchatka Point Formation. It is followed by the most extensive early to middle Eocene MAP with ages enclosed between ~53 and ~43 Ma. The youngest rocks emplaced during this MAP compose of the Mount Wawel and Lions Cove formations (Pańczyk and Nawrocki, 2011*a*, this issue). The next younger magmatic activity phases were recorded by the lava flows or vertical intrusions emplaced in the late Eocene (~37–35 Ma: Mazurek Point Formation–Turret Point–Three Sisters Point area; *op. cit.*), late Oligocene (~28–25 Ma; Blue Dyke and Jardine Peak hypabyssal intrusions; Pańczyk *et al.*, 2009) and late Pliocene to Holocene (Penguin Island volcano; Pańczyk and Nawrocki, 2011*b*, this issue).

The ages of the lowermost lava flows emplaced during the early to middle Eocene MAP decrease gradually from SW (~52 Ma: Paradise Cove) to NE (~48 Ma: Mount Wawel; ~44 Ma: SW King George Bay). This trend seems to continue into the next younger late Eocene MAP represented by the Mazurek Point Formation rocks, cropping out in the NE part of King George Bay (Turret Point–Three Sisters Point area; Fig. 12B, point G). This age migration may reflect the SW–NE direction of accretion of an Eocene island arc forming this part of King George Island (*cf.* Pankhurst and Smellie, 1983; Smellie *et al.*, 1984).

The early to middle Eocene MAP is coeval with abrupt declines of atmospheric CO_2 (Pearson and Palmer, 2000; Pagani *et al.*, 2005) and subsequent gradual climate cooling after the early Eocene climatic optimum and before the abrupt increase in $\delta^{18}O$ at the Eocene/Oligocene boundary (Miller *et al.*, 1991), that reflects the initiation of substantial and permanent ice sheets in Antarctica. It should be stressed that late Eocene and late Oligocene MAP's preceded periods of Antarctic climate cooling recorded by the Polonez and Melville glaciations (Fig. 12; Birkenmajer, 2001). Intense volcanogenic activity could give additional factor (dust thermal isolation) modelling the climate conditions, apart thermal isolation of Antarctica due to opening of the Drake Passage (Livermore *et al.*, 2005; Lagabrielle *et al.*, 2009). This speculative thesis needs, however, more studies focused on volcanic chronology and geochemistry in the worldwide scale.

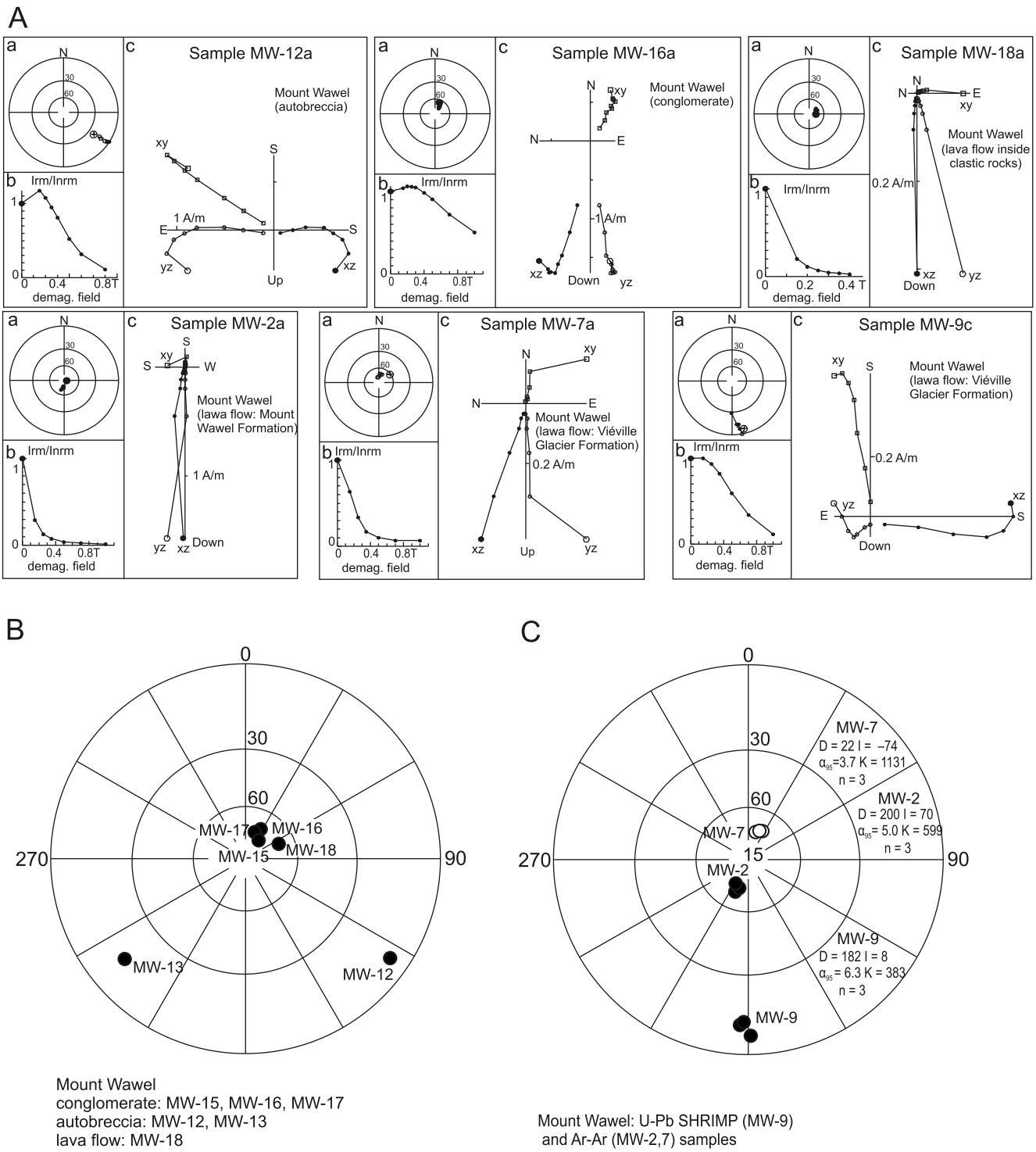

Fig. 11A – typical demagnetisation characteristics (a – demagnetisation paths, b – intensity decay curves and c – orthogonal plots) of` studied igneous rocks from the Mount Wawel section; B – stereographic projections of line-fit mean (on the sample level) palaeomagnetic directions isolated from the Mount Wawel Conglomerate and autobreccia, and the lava flow that separates them; C – stereographic projections of line-fit mean (on the sample level) palaeomagnetic directions isolated from the lava flows of the Mount Wawel section that were subjected of isotope dating; the diagrams were prepared by the means of computer package written by Lewandowski *et al*. (1997)

A: Inrm – intensity of natural remnant magnetisation, Irm – initial intensity of remnant magnetisation; **C**: open (closed) symbols denote upward (downward) pointing inclinations; D, I – mean declination and inclination, α_{95}, K – Fisher's statistics parameters, n – number of specimens

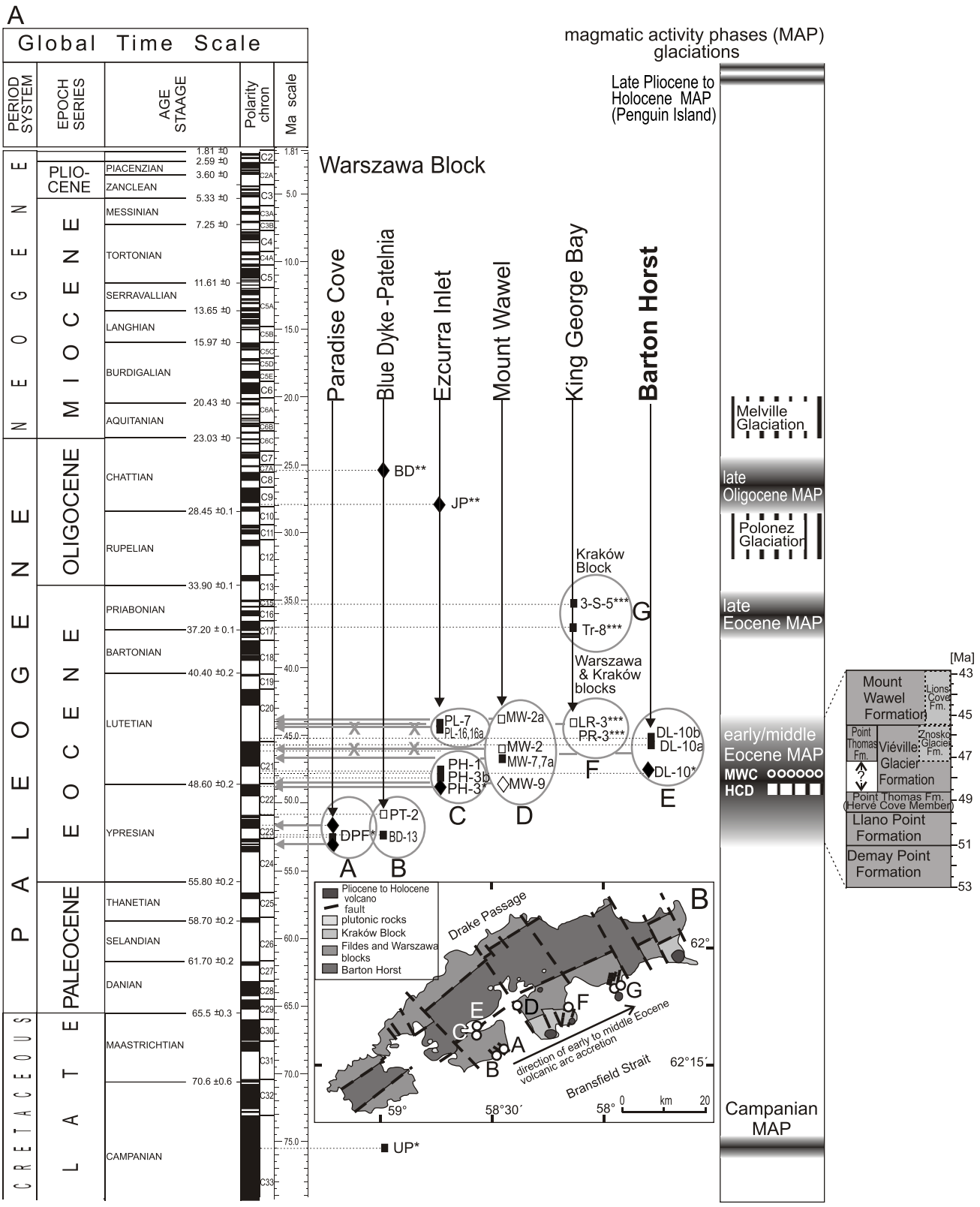

Fig. 12A – U-Pb (rhombus) and $^{40}Ar/^{39}Ar$ (squares) ages of selected magmatic rocks from SE part of King George Island *versus* a stratigraphic chart (after Gradstein *et al*., 2004); B – location of dated sections on the background of structural units of King George Island (after Birkenmajer, 2003)

Open (closed) symbols denote samples with reversed (normal) magnetic polarity; right column presents magmatic activity phases (MAP) distinguished in the area studied and lithostratigraphic units of the early/middle Eocene MAP; MWC – Mount Wawel conglomerate, HCD – Hervé Cove diamictite; * – data according to Nawrocki *et al*. (2010), ** – data according to Pańczyk *et al*. (2009), *** – data presented by Pańczyk and Nawrocki (2011*a*, this issue); A – Paradise Cove (DPF – samples from Demay Point Formation); B – Blue Dyke – Patelnia Peninsula (PT, BD13 – samples from Llano Point Formation), C – Ezcurra Inlet (PH – samples from Hervé Cove Member of Point Thomas Formation, PL – samples from Italian Valley Member of Point Thomas Formation); D – Mount Wawel section (MW-7,9 – samples from Viéville Glacier Formation, MW-2 – samples from Mount Wawel Formation); E – Dufayel Island (DL – samples from Znosko Glacier Formation); F – King George Bay, Lions Rump area; G – King George Bay, Turret Point area; JP – Jardine Peak subvertical intrusion; UP – Uchatka Point Formation; BD – Blue Dyke subvertical intrusion

AGE CONSTRAINTS FOR SELECTED SEDIMENTARY ROCKS OF SE KING GEORGE ISLAND

The early to middle Eocene lavas of SE King George Island contain intercalations of sedimentary rocks. The age of the diamictite exposed among lava flows of the Point Thomas Formation at Hervé Cove in Ezcurra Inlet, regarded speculatively as valley-type tillite recording the oldest traces of Cenozoic glaciers in Antarctica (Birkenmajer *et al.*, 2005), has been recently constrained by magnetostratigraphy and isotopic U-Pb SHRIMP data (Nawrocki *et al.*, 2010). The new ^{40}Ar-^{39}Ar plateau ages support previous age estimations and the general conclusion that the Hervé Cove diamictite immediately postdated the early Eocene climatic optimum.

Another intercalation of sedimentary rocks was found inside the lava flows of the Viéville Glacier Formation during our field works on the western slope of Mount Wawel. This sediment, defined here as the Mount Wawel conglomerate, was deposited in a freshwater environment about 48 Ma ago. The freshwater provenance of the conglomerate can be inferred from the chemical composition of chabazite (e.g., Johnson and Smellie, 2007; Smellie, 2008) that was found in the bottom part of the lava flow covering the conglomerate and autobreccia (Figs. 5 and 6). The Mount Wawel conglomerate indicates that deep valleys of mountain rivers developed in this part of King George Island *ca*. 48 Ma ago. The glacial provenance of the Hervé Cove diamictite should be therefore more carefully proven. It can not be excluded that this sediment might represent a mountain river environment as well.

The Eocene magma of the Znosko and Viéville Glacier formations was contaminated by zircon grains derived from much older Ordovician sediment. Four analyses of small rounded zircon grains from the Znosko Glacier Formation gave ages of 467–497 Ma (Nawrocki *et al.*, 2010). One study of such a rounded grain from the Viéville Glacier Formation gave a similar age of 497 Ma (Table 2). These zircons were most probably inherited from rocks affected by the Ross Orogeny, and their possible source could be located in the area of Ellsworth Mountains. Another, less probable source might be linked with a deep basement of South Shetland Islands and tectonic structures of South America that could supply northern part of Antarctic Peninsula with detrital material.

CONCLUSIONS

1. Five magmatic activity phases have been distinguished in the SE coast of King George Island. The oldest, Late Cretaceous (Campanian) phase is represented by basalts of the Uchatka Point Formation (Nawrocki *et al*., 2010) and is followed by an early to middle Eocene phase (~53–43 Ma) with lava flow ages decreasing from SW to NE, a younging trend similar to that previously identified for the whole South Shetland Islands (Pankhurst and Smellie, 1983; Smellie *et al*., 1984). The next younger magmatic activity phases apparently continue this younging trend and were recorded by lava flows and hypabyssal intrusions emplaced in the late Eocene (~37–35 Ma), late Oligocene (~28–25 Ma) and late Pliocene to Holocene. The early to middle Eocene magmatic activity phase was the most extensive, producing the largest volume of magma in the study area.

2. The new isotopic ages controlled by magnetostratigraphy substantially refine the existing stratigraphic chart of SE King George Island. The Demay Point Formation was emplaced between ~53 and ~51 Ma. It was followed by the Llano Point Formation whose age is enclosed between ~51 and ~49.5 Ma. Assuming continuity of the section exposed along the NW coast of Ezcurra Inlet, we conclude that the whole volcanogenic succession in the Ezcurra Inlet i.e. the Point Thomas Formation was deposited between ~49.4 and ~45.4 Ma. Both units forming the Mount Wawel section i.e. the Viéville Glacier and Mount Wawel formations were emplaced between ~48.6 and ~42.8 Ma.

3. Speculatively, intense volcanic activity could be a factor forcing climate conditions in the late Eocene, immediately prior to the thermal isolation of Antarctica due to opening of Drake Passage.

4. The new ^{40}Ar-^{39}Ar plateau ages support the previous age estimations and general conclusion that the Hervé Cove diamictite immediately postdated the early Eocene climatic optimum. Another coarse-grained sediment defined here as the Mount Wawel conglomerate was deposited in a freshwater environment about 48 Ma ago indicating that deep mountain valleys developed at that time. The glacial origin of the Hervé Cove diamictite should be therefore more carefully proven because it might represent a mountain river environment as well.

Acknowledgements. This study was supported by the grants of the Polish Ministry of Science and Higher Education (No N N307 058434 and ACE IPY 54 grant). The field work was carried out during the 31st and 33rd Polish Antarctic Expedition to the Arctowski Station. We thank A. Tatur, K. Krajewski, K. Chwedorzewska and M. Korczak for support during the field work. We are grateful to E. Krzemińska, L. Giro K. Dymna and G. Zieliński for analytical work. We are grateful for helpful reviews from J. Smellie and K. Birkenmajer. Special thanks go to A. Scherstén from Lund University for Ar-Ar analysis.

REFERENCES

BIRKENMAJER K. (1981) – Lithostratigryphy of the Point Hennequin Group (Miocene volcanics and sediments) at King George Island (South Shetland Islands, Antarctica). Stud. Geol. Pol., **72**: 59–73.

BIRKENMAJER K. (1989) – A guide to Tertiary geochronology of King George Island, West Antarctica. Pol. Polar Res., **10** (4): 555–579.

BIRKENMAJER K. (2001) – Mesozoic and Cenozoic stratigraphic units in parts of the South Shetland Islands and Northern Antarctic Peninsula (as used by the Polish Antarctic Programmes). In: Geological Results of the Polish Antarctic Expeditions. Part XIII (ed. K. Birkenmajer). Stud. Geol. Pol., **118**.

BIRKENMAJER K. (2002) – Admiralty Bay, King George Island, South Shetland Islands, West Antarctica. Geological map 1:50 000. Pol. Acad. Sc.

BIRKENMAJER K. (2003) – Admiralty Bay, King George Island (South Shetland Islands, West Antarctica): a geological monograph. In: Geological Results of the Polish Antarctic Expeditions. Part XIV (ed. K. Birkenmajer). Stud. Geol. Pol., **120**.

BIRKENMAJER K., DELITALA M. C., NARĘBSKI W., NICOLETTI M. and PETRUCCIANI C. (1986) – Geochronology of Tertiary island-arc volcanics and glacigenic deposits, King George Island, South Shetlands Islands (West Antarctica). Bull. Acad. Pol. Ser. Sc. Terre., **34**: 257–273.

BIRKENMAJER K., GAŹDZICKI A., KRAJEWSKI K. P., PRZYBYCIN A., SOLECKI A., TATUR A. and YOON H. I. (2005) – First Cenozoic glaciers in West Antarctica. Pol. Polar Res., **26** (1): 3–12.

BIRKENMAJER K., NARĘBSKI W., NICOLETTI M. and PETRUCCIANI C. (1983*a*) – K-Ar ages of "Jurassic volcanics" and "Andean" intrusions of King George Island South Shetland Islands (West Antarctica). Bull. Acad. Pol. Sc., Sér. Sc. Terre, Sc., **30** (3–4): 121–131.

BIRKENMAJER K., NARĘBSKI W., NICOLETTI M. and PETRUCCIANI C. (1983*b*) – Late Cretaceous through Late Oligocene K-Ar ages of the King George Island Supergroup volcanics, South Shetland Islands (West Antarctica). Bull. Acad. Pol. Sc., Sér. Sc. Terre, Sc., **30**: 133–143.

DALRYMPLE G. B. and LAPHERE M. A. (1971) – $^{40}Ar/^{39}Ar$ technique of K-Ar dating: a comparison with the conventional technique. Earth Planet. Sc. Lett., **12**: 300–308.

GRADSTEIN F. M., OGG J. G. and SMITH A. (2004) – Geological Time Scale 2004. Cambridge University Press, Cambridge.

JOHNSON J. S. and SMELLIE J. L. (2007) – Zeolite compositions as proxies for eruptive paleoenvironoment. Geochem., Geoph., Geosystem, **8**: doi: 10.1029/2006GC001450

KIRSCHVINK J. L. (1980) – The least square line and plane and the analysis of paleomagnetic data. Geoph. J. Royal Astr. Soc., **62**: 699–718.

KRAUS S. (2005) – Magmatic dyke systems of the South Shetland Islands volcanic arc (West Antarctica): reflections of the geodynamic history. Dissertation, LMU Munich: Faculty of Geosciences. http://nbn-resolving.de/urn:nbn:de:bvb:19-38277

KRAUS S., McWILLIAMS M. and PECSKAY Z. (2007) – New $^{40}Ar/^{39}Ar$ and K/Ar ages of dikes in the South Shetland Islands (Antarctic Peninsula). In: Antarctica: a Keystone in a Changing World – Online Proceedings of the 10th ISAES, USGS Open-File Report 2007-1047 (eds. A. K. Cooper and C. R. Raymond). Short Research Paper 035.

KRETZ R. (1983) – Symbols for rock-forming minerals. Am. Miner., **68**: 277–279.

LAGABRIELLE Y., GODDÉRIS Y., DONNADIEU Y., MALAVIEILLE J. and SUAREZ M. (2009) – The tectonic history of Drake Passage and its possible impacts on global climate. Earth Planet. Sc. Lett., **279**: 197–211.

Le MAITRE R. W., BATEMAN P., DUDEK A., KELLER J., LAMEYRE J., Le BAS M., SABINE P. A., SCHMID R., SORENSEN H., STRECKEISEN A., WOOLEY A. R. and ZANETTIN B. (1989) – A classification of igneous rocks and glossary of terms. Recommendations of the International Union of Geological Sciences Subcommission on the Systematics of Igneous Rocks. Blackwell, Oxford.

LEWANDOWSKI M., WERNER T. and NOWOŻYŃSKI K. (1997) – PCA – a package of Fortran programs for paleomagnetic data analysis. Instit. Geophys., Pol. Acad. Sc., Manuscript.

LIVERMORE R., NANKIVELL A., EAGLES G. and MORRIS P. (2005) – Paleogene opening of Drake Passage. Earth Planet. Sc. Lett., **236**: 459–470.

MILLER K. G., WRIGHT J. D. and FAIRBANKS R. G. (1991) – Unlocking the icehouse: Oligocene–Miocene oxygen isotope, eustasy, and margin erosion. J. Geophys. Res., **96**: 6829–6848.

NAWROCKI J., PAŃCZYK M. and WILLIAMS I. S. (2010) – Isotopic ages and palaeomagnetism of selected magmatic rocks from King George Island (Antarctic Peninsula). J. Geol. Soc. London, **167**: 1063–1079.

PAGANI M., ZACHOS J. C., FREEMAN K. H., TRIPPLE B. and BOHATY S. (2005) – Marked decline in atmospheric carbon dioxide concentrations during the Paleogene. Science, **309**: 600–603.

PANKHURST R. J. and SMELLIE J. L. (1983) – K-Ar geochronology of the South Shetland Islands, Lesser Antarctica: apparent lateral migration of Jurassic to Quaternary island arc volcanism. Earth Planet. Sc. Lett., **66**: 214–222.

PAŃCZYK M., NAWROCKI J. and WILLIAMS I. S. (2009) – Isotope age constraint for the Blue Dyke and Jardine Peak subvertical intrusions of King George Island, West Antarctica. Pol. Polar Res., **30**: 379–391.

PAŃCZYK M. and NAWROCKI J. (2011*a*) – Geochronology of selected andesitic lavas from the King George Bay area (SE King George Island). Geol. Quart., **55** (4): 323–334.

PAŃCZYK M. and NAWROCKI J. (2011*b*) – Pliocene age of the oldest basaltic rocks of Penguin Island (South Shetland Islands, northern Antarctic Peninsula). Geol. Quart., **55** (4): 335–344.

PEARSON P. N. and PALMER M. R. (2000) – Atmospheric carbon dioxide concentrations over the past 60 million years. Nature, **406**: 695–699.

RENNE P. R., DEINO A. L., WALTER R. C., TURRIN B. D., SWISHER C. C., BECKER T. A., CURTIS G. H., SHARP W. D. and JAOUNI A. R. (1994) – Intercalibration of astronomical and radioisotopic time. Geology, **22**: 783–786.

SMELLIE J. L. (2008) – Basaltic subglacial sheet-like sequences: evidence for two types with different implications for the inferred thickness of associated ice. Earth. Sc. Rev., **88**: 60–88.

SMELLIE J. L., MILLAR I. L., REX D. C. and BUTTERWORTH P. J. (1998) – Subaqueous, basaltic lava dome and carapace breccia on King George Island, South Shetland Islands, Antarctica. Bull. Volcanol., **59**: 245–261.

SMELLIE J. L., PANKHURST R. J., THOMSON M. R. A. and DAVIES R. E. S. (1984) – The geology of the South Shetland Islands: VI. Stratigraphy, geochemistry and evolution. Br. Antarct. Surv. Sc. Rep., **87**.

STEIGER R. H. and JÄGER E. (1977) – Subcommission on geochronology: convention on the use of decay constants in geo- and cosmochronology. Earth Planet. Sc. Lett., **36**: 359–362.

TROEDSON A. L. and RIDING J. B. (2002) – Upper Oligocene to lowermost Miocene strata of King George Island, South Shetland Islands, Antarctica: stratigraphy, facies analysis and implications for the glacial history of the Antarctic Peninsula. J. Sed. Res., **72**: 510–523.

TROEDSON A. L. and SMELLIE J. L. (2002) – The Polonez Cove Formation of King George Island, Antarctica: stratigraphy, facies and implications for mid-Cenozoic cryosphere development. Sedimentology, **49**, 277–301.

WILLAN R. C. R. and ARMSTRONG D. C. (2002) – Successive geothermal, volcanic-hydrothermal and contact-metasomatic events in Cenozoic volcanic-arc basalts, South Shetland Islands, Antarctica. Geol. Mag., **139**: 209–231.

WILLIAMS I. S. and CLAESSON S. (1987) – Isotopic evidence for the Precambrian provenance and Caledonian metamorphism of high grade paragneisses from the Seve Ns , Scandinavian Caledonides: II Ion microprobe zircon U-Th-Pb. Contribut. Miner. Petrol., **97**: 205–217.

WINCHESTER J. A. and FLOYD P. A. (1977) – Geochemical discrimination of different magma series and their differentiation products using immobile elements. Chem. Geol., **20**– 325–343.

ZIJDERVELD J. D. A. (1967) – AC demagnetization of rocks: analysis of results. In: Methods in Paleomagnetism (eds. D. W. Collinson *et al.*): 254–287. Elsevier, New York.

APPENDIX

$^{40}Ar/^{39}Ar$ analytical data of the King George igneous rocks

Run ID	Pwr/T°C	Ca/K	$^{36}Ar/^{39}Ar$	$\%^{36}Ar(Ca)$	$^{40}*Ar/^{39}Ar$	Mol ^{39}Ar $x10^{-14}$	% Step	Cum. %	$\%^{40}Ar*$	Age [Ma]	±Age
PT-2 (J = 0.0060878 ±5.500000e-6)											
1826-01A	•2.0	2.31021	0.145816	0.2	4.66953	0.0636	5.9	5.9	9.8	50.56941	2.11206
1826-01B	•2.1	2.98929	0.065042	0.6	4.90366	0.0603	5.6	11.4	20.4	53.06798	1.57751
1826-01C	•2.3	3.85039	0.056488	0.9	4.57588	0.105	9.7	21.1	21.6	49.56896	1.18417
1826-01D	•2.5	4.26487	0.040371	1.4	4.74371	0.1341	12.3	33.4	28.7	51.36136	0.847
1826-01E	•2.7	3.71015	0.03362	1.5	4.80619	0.0969	8.9	42.3	32.9	52.02823	1.00237
1826-01F	•2.9	5.01521	0.027065	2.5	4.64285	0.1497	13.8	56.1	37.3	50.28445	0.67352
1826-01G	•3.1	6.14795	0.026104	3.2	4.48089	0.0541	5	61.1	37.4	48.55369	1.51579
1826-01H	3.3	5.19459	0.02622	2.7	4.35793	0.0589	5.4	66.5	36.6	47.23861	1.37795
1826-01I	3.5	6.76909	0.027605	3.3	4.45344	0.0815	7.5	74	36	48.26025	1.04764
1826-01J	3.7	6.62247	0.03151	2.8	4.01583	0.0509	4.7	78.7	30.7	43.57483	1.5479
1826-01K	4	8.29107	0.040543	2.8	4.10643	0.0518	4.8	83.5	26	44.54582	1.69209
1826-01L	4.5	7.8751	0.048582	2.2	4.12137	0.0651	6	89.5	22.6	44.70591	1.39238
1826-01M	6	7.71155	0.064672	1.6	4.22961	0.1143	10.5	100	18.3	45.86523	1.13242
Integ. age =										48.9	1
(•) Plateau age =							61.1			50.8	1.2
PL-16 (J = 0.0060878 ±5.500000e-6)											
1827-01A	2	1.56545	0.127136	0.2	4.91771	0.1137	8.2	8.2	11.6	53.21786	1.52635
1827-01B	2.1	1.54617	0.048046	0.4	4.69355	0.0687	4.9	13.1	24.9	50.82583	1.44658
1827-01C	2.3	1.85968	0.036573	0.7	4.69287	0.1086	7.8	20.9	30.4	50.8186	0.95256
1827-01D	2.5	2.42594	0.025892	1.3	4.46755	0.1073	7.7	28.6	37.1	48.41109	0.84349
1827-01E	2.7	1.45974	0.013096	1.5	4.46383	0.157	11.3	39.9	53.9	48.37127	0.52753
1827-01F	2.9	1.58133	0.008233	2.6	4.34532	0.0801	5.7	45.6	64.7	47.1037	0.79887
1827-01G	•3.1	1.88317	0.008245	3.1	4.22335	0.1145	8.2	53.8	64.1	45.79824	0.57697
1827-01H	•3.3	1.61611	0.007172	3	4.18314	0.0769	5.5	59.3	67	45.36757	0.80728
1827-01I	•3.5	1.88228	0.007309	3.5	4.12889	0.0999	7.2	66.5	66.4	44.78649	0.65577
1827-01J	•3.7	1.60178	0.007289	3	4.11544	0.075	5.4	71.9	66.3	44.64237	0.86274
1827-01K	•4.0	1.44447	0.006865	2.8	4.22067	0.0842	6	77.9	68.1	45.76954	0.71722
1827-01L	•4.5	2.35786	0.007287	4.4	4.08507	0.0969	7	84.9	66.5	44.31692	0.66636
1827-01M	•6.0	2.8192	0.008619	4.4	4.08911	0.2106	15.1	100	62.7	44.36028	0.38127
Integ. age =										47.1	0.6
(•) Plateau age =							54.4			44.9	0.7
PL-16a (J = 0.0060878 ±5.500000e-6)											
1827-02A	2	1.47138	0.051528	0.4	4.68664	0.1868	8.8	8.8	23.6	50.75206	0.7358
1827-02B	2.1	1.70805	0.017322	1.3	4.53208	0.1158	5.5	14.3	47.3	49.10096	0.67629
1827-02C	2.3	1.87166	0.011821	2.1	4.47087	0.1875	8.8	23.1	56.6	48.44661	0.42224
1827-02D	2.5	1.50797	0.008662	2.3	4.28647	0.2105	9.9	33	63.1	46.47396	0.35337
1827-02E	2.7	1.26019	0.006231	2.7	4.32957	0.2022	9.5	42.6	70.7	46.93522	0.35704
1827-02F	2.9	0.99165	0.005945	2.2	4.32769	0.1286	6.1	48.6	71.6	46.91508	0.51338
1827-02G	3.1	1.09989	0.005897	2.5	4.29156	0.1152	5.4	54.1	71.6	46.52838	0.55474
1827-02H	•3.3	0.91838	0.005935	2.1	4.10399	0.0983	4.6	58.7	70.5	44.51967	0.62727
1827-02I	•3.5	1.4206	0.005873	3.3	4.1818	0.1191	5.6	64.3	71.3	45.35326	0.59174
1827-02J	•3.7	1.38985	0.006416	2.9	4.11694	0.1038	4.9	69.2	69.1	44.65841	0.53314
1827-02K	•4.0	1.55043	0.007152	2.9	4.10478	0.075	3.5	72.7	66.7	44.52811	0.71007
1827-02L	•4.5	1.55332	0.007449	2.8	4.09899	0.153	7.2	79.9	65.7	44.46613	0.39854
1827-02M	•6.0	1.36322	0.007887	2.3	4.10115	0.4256	20.1	100	64.3	44.48928	0.22353
Integ. age =										46.4	0.4
(•) Plateau age =							45.9			44.6	0.4

App. cont.

Run ID	Pwr/T°C	Ca/K	$^{36}Ar/^{39}Ar$	$\%^{36}Ar(Ca)$	$^{40}*Ar/^{39}Ar$	Mol ^{39}Ar $x10^{-14}$	% Step	Cum. %	$\%^{40}Ar*$	Age [Ma]	±Age
PH-3b (J = 0.0060878 ±5.500000e-6											
1828-02A	2	0.23768	0.092074	0	3.64798	0.2264	7.7	7.7	11.8	39.6268	1.03061
1828-02B	2.1	0.30129	0.035174	0.1	4.29399	0.1356	4.6	12.3	29.3	46.55443	0.67405
1828-02C	2.3	0.33292	0.022304	0.2	4.47513	0.2405	8.2	20.5	40.5	48.49216	0.42393
1828-02D	2.5	0.3854	0.013457	0.4	4.54465	0.278	9.5	30	53.4	49.23524	0.33192
1828-02E	2.7	0.36883	0.009083	0.5	4.58001	0.2494	8.5	38.5	63.2	49.61313	0.31002
1828-02F	•2.9	0.30529	0.00783	0.5	4.48429	0.3796	12.9	51.4	66.1	48.59006	0.25243
1828-02G	•3.1	0.49746	0.006935	1	4.45229	0.2824	9.6	61	68.7	48.24793	0.29853
1828-02H	•3.3	0.4151	0.007956	0.7	4.46394	0.1968	6.7	67.8	65.7	48.37246	0.37631
1828-02I	•3.5	0.95428	0.010905	1.2	4.40636	0.1752	6	73.7	58	47.75677	0.4543
1828-02J	•3.7	0.66874	0.007902	1.1	4.4744	0.1124	3.8	77.6	66	48.48432	0.45932
1828-02K	•4.0	0.44932	0.007405	0.8	4.35121	0.1075	3.7	81.2	66.7	47.16678	0.47565
1828-02L	•4.5	0.57111	0.006823	1.1	4.40196	0.1447	4.9	86.1	68.8	47.70963	0.36474
1828-02M	•5.2	0.67605	0.009352	1	4.38386	0.1823	6.2	92.4	61.6	47.51606	0.34422
1828-02N	•6.0	0.52149	0.011542	0.6	4.4196	0.2243	7.6	100	56.6	47.89838	0.31465
Integ. age =										47.6	0.4
(•) Plateau age =							61.5			48.1	0.2
PH-3b Plagioclaze (J = 0.0060878 ±5.500000e-6)											
1838-01C	2.3	0.19634	0.132664	0	4.29849	0.0142	1.6	1.6	9.9	46.60258	4.86976
1838-01D	2.5	0.22791	0.06561	0	3.53908	0.0208	2.4	4.1	15.4	38.45639	2.90519
1838-01E	2.7	0.19211	0.029075	0.1	2.79791	0.0266	3.1	7.1	24.6	30.47028	2.9341
1838-01F	2.9	0.2348	0.019432	0.2	2.83507	0.0261	3	10.2	33.1	30.87155	1.68583
1838-01G	3.1	0.14645	0.018744	0.1	4.13042	0.0621	7.2	17.4	42.7	44.80287	1.31181
1838-01H	•3.3	0.07667	0.006864	0.2	3.82228	0.0512	5.9	23.3	65.4	41.49861	0.8743
1838-01I	•3.5	0.13695	0.006457	0.3	3.99076	0.0487	5.6	29	67.7	43.30604	0.92717
1838-01J	•3.7	0.09891	0.00839	0.2	3.72607	0.0905	10.5	39.5	60.1	40.46565	0.50484
1838-01K	•4.0	0.12027	0.006775	0.2	3.95744	0.1252	14.5	54	66.4	42.94875	0.62411
1838-01L	•5.0	0.08451	0.004466	0.3	3.78121	0.2456	28.5	82.5	74.2	41.05779	0.32047
1838-01M	•6.0	0.05632	0.005631	0.1	3.86009	0.1506	17.5	100	69.9	41.90438	0.36432
Integ. age =										41.2	0.5
(•) Plateau age =							82.6			41.5	0.8
DL-10a (J = 0.0061013 ±5.400000e-6)											
1835-01A	2	0.02715	0.098718	0	3.08629	0.3475	2.7	2.7	9.6	33.65557	1.04879
1835-01B	2.1	0.04364	0.027058	0	3.93421	0.2898	2.3	5	33	42.7931	0.41962
1835-01C	2.3	0.02406	0.023237	0	3.99033	0.4441	3.5	8.4	36.8	43.39623	0.33858
1835-01D	2.5	0.01285	0.010119	0	4.05021	0.5548	4.3	12.7	57.5	44.03958	0.20888
1835-01E	•2.7	0.00779	0.005971	0	4.17642	0.83	6.5	19.2	70.3	45.39482	0.13973
1835-01F	•2.9	0.00723	0.003441	0	4.24575	0.9007	7	26.2	80.7	46.13886	0.10406
1835-01G	•3.1	0.00536	0.003004	0	4.13907	1.2992	10.1	36.3	82.3	44.99386	0.13306
1835-01H	•3.3	0.00218	0.002202	0	4.25719	1.0889	8.5	44.7	86.7	46.26153	0.09211
1835-01I	•3.5	0.00287	0.002047	0	4.19337	1.0027	7.8	52.5	87.4	45.57677	0.09583
1835-01J	•3.7	0.00262	0.002046	0	4.17122	1.0198	7.9	60.5	87.3	45.33904	0.09321
1835-01K	•4.0	0.00376	0.002343	0	4.13624	0.9964	7.7	68.2	85.6	44.96351	0.09805
1835-01L	•4.5	0.00472	0.002523	0	4.15403	1.3185	10.2	78.5	84.8	45.15444	0.08854
1835-01M	•5.2	0.0079	0.002711	0	4.16162	1.5802	12.3	90.7	83.9	45.23599	0.09508
1835-01N	•6.0	0.01017	0.002802	0	4.17503	1.1917	9.3	100	83.4	45.37994	0.09664
Integ. age =										44.91	0.2
(•) Plateau age =							87.3			45.5	0.3

App. cont.

Run ID	Pwr/T°C	Ca/K	$^{36}Ar/^{39}Ar$	$\%^{36}Ar(Ca)$	$^{40}*Ar/^{39}Ar$	Mol ^{39}Ar x10^{-14}	% Step	Cum. %	$\%^{40}Ar*$	Age [Ma]	±Age
DL-10b (J = 0.0061013 ±5.400000e-6)											
1835-02A	2	0.01669	0.120519	0	3.33709	0.2552	1.9	1.9	8.6	36.36314	1.23613
1835-02B	2.1	0.0207	0.069184	0	3.57822	0.2469	1.8	3.7	14.9	38.96246	0.80922
1835-02C	2.3	0.0197	0.032399	0	3.82985	0.396	2.9	6.6	28.6	41.67101	0.4262
1835-02D	2.5	0.00929	0.01756	0	3.97234	0.5722	4.2	10.8	43.4	43.20297	0.26583
1835-02E	2.7	0.02233	0.008014	0	4.06734	1.1279	8.3	19.2	63.2	44.22361	0.12927
1835-02F	•2.9	0.00604	0.004888	0	4.19129	0.8023	5.9	25.1	74.4	45.55445	0.13199
1835-02G	•3.1	0.01176	0.004256	0	4.13656	1.3453	9.9	35	76.7	44.96689	0.09627
1835-02H	•3.3	0.00894	0.004125	0	4.16275	1.14	8.4	43.4	77.3	45.2481	0.10423
1835-02I	•3.5	0.01338	0.002907	0.1	4.1269	1.0051	7.4	50.8	82.8	44.86322	0.09776
1835-02J	•3.7	0.01154	0.002786	0.1	4.13877	1.056	7.8	58.6	83.4	44.99063	0.10307
1835-02K	•4.0	0.01163	0.002851	0.1	4.14603	1.0571	7.8	66.4	83.1	45.06855	0.09809
1835-02L	•4.5	0.0207	0.003006	0.1	4.10841	1.3881	10.2	76.7	82.2	44.66468	0.0924
1835-02M	•5.2	0.00532	0.002839	0	4.15562	1.7124	12.6	89.3	83.2	45.17152	0.08699
1835-02N	•6.0	0.00738	0.002937	0	4.12941	1.4477	10.7	100	82.6	44.89017	0.09584
Integ. age =										44.5	0.2
(•) Plateau age =							80.8			45.02	0.19
BD-13 (J = 0.0060815 ±5.600000e-6)											
1831-01A	2	0.25217	0.076548	0	3.95229	0.2378	8.9	8.9	14.9	42.84956	0.87474
1831-01B	•2.1	0.29817	0.029271	0.1	4.7494	0.1477	5.5	14.4	35.5	51.36964	0.60146
1831-01C	•2.3	0.37413	0.022529	0.2	4.82629	0.2702	10.1	24.4	42.1	52.18937	0.36552
1831-01D	•2.5	0.29809	0.015605	0.3	4.88602	0.2931	10.9	35.3	51.5	52.82589	0.30839
1831-01E	•2.7	0.22816	0.010554	0.3	4.87519	0.3892	14.5	49.8	61	52.7105	0.24913
1831-01F	•2.9	0.27354	0.00859	0.4	4.83599	0.2273	8.5	58.3	65.7	52.2928	0.3157
1831-01G	•3.1	0.35573	0.007321	0.7	4.78882	0.2022	7.5	65.8	69	51.78997	0.28197
1831-01H	3.3	0.37936	0.007223	0.7	4.69636	0.1764	6.6	72.4	68.9	50.80396	0.34199
1831-01I	3.5	0.67422	0.008885	1	4.55998	0.1819	6.8	79.2	63.7	49.34865	0.32836
1831-01J	3.7	0.52131	0.008568	0.8	4.59284	0.1381	5.1	84.3	64.6	49.69948	0.39841
1831-01K	4	0.75201	0.005325	1.9	5.15071	0.1164	4.3	88.7	76.9	55.644	0.41859
1831-01L	4.5	0.89488	0.008485	1.4	4.40767	0.1658	6.2	94.8	64.1	47.72192	0.34124
1831-01M	5.2	0.96228	0.009286	1.4	4.41825	0.0789	2.9	97.8	62	47.83498	0.66545
1831-01N	6	1.01388	0.0107	1.3	4.3194	0.0596	2.2	100	58	46.77855	0.85052
Integ. age =										50.7	0.4
(•) Plateau age =							57			52.3	0.5
MW-7a (J = 0.0060878 ±5.500000e-6)											
1829-01A	2	0.39808	0.115035	0	3.41297	0.2101	4	4	9.1	37.10006	1.21022
1829-01B	2.1	0.37824	0.042818	0.1	4.1422	0.1667	3.2	7.2	24.7	44.92908	0.66976
1829-01C	2.3	0.42233	0.0288	0.2	4.21641	0.3462	6.6	13.8	33.2	45.72393	0.42924
1829-01D	•2.5	0.28034	0.017861	0.2	4.34904	0.6594	12.5	26.3	45.2	47.14354	0.24432
1829-01E	•2.7	0.30607	0.00847	0.5	4.34295	0.748	14.2	40.5	63.5	47.07837	0.17266
1829-01F	•2.9	0.41997	0.006976	0.8	4.31828	0.668	12.7	53.3	67.9	46.81438	0.16079
1829-01H	•3.3	0.54121	0.004274	1.7	4.27591	0.4048	7.7	61	77.5	46.36093	0.19476
1829-01I	•3.5	0.69756	0.004351	2.2	4.30037	0.4485	8.5	69.5	77.4	46.6227	0.18751
1829-01J	•3.7	0.58914	0.004189	1.9	4.32423	0.3358	6.4	75.9	78.1	46.87803	0.23846
1829-01K	4	0.59245	0.003976	2	4.2681	0.3322	6.3	82.2	78.7	46.27734	0.221
1829-01L	4.5	1.83826	0.005873	4.2	4.11287	0.3681	7	89.2	71.2	44.61486	0.22843
1829-01M	5.2	0.97035	0.006587	2	3.99691	0.3547	6.8	96	67.7	43.37198	0.21204
1829-01N	6	0.47132	0.005519	1.2	4.19334	0.2124	4	100	72.2	45.47679	0.31799
Integ. age =										45.9	0.3
(•) Plateau age =							62.1			46.8	0.3

App. cont.

Run ID	Pwr/T°C	Ca/K	$^{36}Ar/^{39}Ar$	$\%^{36}Ar(Ca)$	$^{40}*Ar/^{39}Ar$	Mol ^{39}Ar $x10^{-14}$	% Step	Cum. %	$\%^{40}Ar*$	Age [Ma]	±Age
MW-7b (J = 0.0060878 ± 5.500000e-6)											
1829-02A	2	0.29838	0.154389	0	3.18927	0.1433	3.3	3.3	6.5	34.69156	1.68312
1829-02B	2.1	0.2272	0.052329	0.1	4.12611	0.1234	2.8	6.1	21.1	44.75675	0.88765
1829-02C	2.3	0.24214	0.033167	0.1	4.20534	0.2681	6.2	12.3	30	45.60537	0.50401
1829-02D	•2.5	0.22961	0.015088	0.2	4.28968	0.3431	7.9	20.2	49.1	46.50824	0.29296
1829-02E	•2.7	0.1687	0.008898	0.3	4.27387	0.6111	14.1	34.3	62	46.33911	0.18217
1829-02F	•2.9	0.20552	0.005391	0.5	4.31967	0.4176	9.6	43.9	73.1	46.82923	0.18888
1829-02G	•3.1	0.24938	0.004792	0.7	4.33016	0.3857	8.9	52.8	75.5	46.94152	0.20018
1829-02H	•3.3	0.23914	0.004221	0.8	4.30563	0.3275	7.5	60.3	77.7	46.67897	0.20481
1829-02I	•3.5	0.23843	0.003696	0.9	4.33452	0.3838	8.8	69.2	80	46.98816	0.18184
1829-02J	3.7	0.25206	0.00332	1	4.28379	0.2485	5.7	74.9	81.5	46.44526	0.25389
1829-02K	4	0.29073	0.003528	1.1	4.25063	0.2601	6	80.9	80.5	46.09033	0.232
1829-02L	4.5	0.36326	0.003804	1.3	4.24091	0.2964	6.8	87.7	79.3	45.98623	0.20725
1829-02M	5.2	0.24265	0.003746	0.9	4.22554	0.2929	6.7	94.5	79.4	45.82169	0.18809
1829-02N	6	0.75251	0.003826	2.6	4.18759	0.2397	5.5	100	79.2	45.41526	0.23129
Integ. age =										45.9	0.3
(•) Plateau age =							56.9			46.7	0.3

$^{40}Ar/^{39}Ar$ Step-Heating Data for Run 1900-01; PL-7													
Run ID	Status	Watts	Ca/K	Cl/K	$^{36}Ar/^{39}Ar$	$\%^{36}Ar(Ca)$	$^{40}*Ar/^{39}Ar$	Mol ^{39}Ar	% Step	Cum. %	$\%^{40}Ar*$	Age [Ma]	±Age
PL-7 (J = 0.005959 ±5.700000e-6)													
•1900-01A	0	0	4.86191	0	0.195629	0.3	4.32331	0.0679	5.3	5.3	7	45.88917	5.23742
•1900-01B	0	0	17.48904	0	0.057311	3.6	3.85277	0.3365	26.1	31.3	19	40.9509	1.4457
•1900-01C	0	0	14.12543	0	0.013661	12	4.1667	0.2556	19.8	51.1	53.9	44.24698	1.11196
•1900-01D	0	0	27.91675	0	0.025248	12.9	4.28976	0.2232	17.3	68.4	39.6	45.53748	1.04596
1900-01E	0	0	46.09734	0	0.030669	17.5	2.65354	0.1293	10	78.4	25.9	28.30364	1.37645
1900-01F	0	0	40.34368	0	0.031759	14.8	2.72238	0.129	10	88.4	25.2	29.03212	1.61019
1900-01G	0	0	53.04702	0	0.024747	24.9	4.56209	0.1503	11.6	100	45	48.38997	1.37528
Integ. age =												41.1	1.4
(•) Plateau age =									68.4			44.1	1.3
$^{40}Ar/^{39}Ar$ Step-Heating Data for Run 1903-01; Ph-1													
Ph-1 (J = 0.005959 ±5.700000e-6)													
1903-01A	0	0	4.88396	0	0.050848	1.1	6.46468	0.2722	9.3	9.3	30.3	68.19326	1.20862
1903-01B	0	0	7.82446	0	0.012179	7.5	5.47261	0.4297	14.7	24.1	62.1	57.8943	0.64104
•1903-01C	0	0	7.57891	0	0.00631	14	4.8026	0.4787	16.4	40.5	74.9	50.90537	0.48965
•1903-01D	0	0	8.13522	0	0.005415	17.5	4.51075	0.4111	14.1	54.6	77.3	47.85253	0.4007
•1903-01E	0	0	11.22256	0	0.006549	19.9	4.43922	0.2706	9.3	63.9	74.1	47.10347	0.65539
•1903-01F	0	0	13.12883	0	0.005817	26.3	4.4464	0.1769	6.1	70	77.7	47.17869	0.48613
•1903-01G	0	0	16.46791	0	0.006621	28.9	4.50367	0.1997	6.9	76.8	76.3	47.77842	0.4233
•1903-01H	0	0	31.52152	0	0.010016	36.6	4.58953	0.277	9.5	86.3	70.8	48.67713	0.75353
•1903-01I	0	0	31.79669	0	0.010891	34	4.40139	0.3983	13.7	100	67.2	46.70724	0.58681
Integ. age =												51.5	0.5
(•) Plateau age =									59.5			47.6	0.4

App. cont.

$^{40}Ar/^{39}Ar$ Step-Heating Data for Run 1905-01; MW-2a													
Run ID	Status	Watts	Ca/K	Cl/K	$^{36}Ar/^{39}Ar$	$\%^{36}Ar(Ca)$	$^{40}*Ar/^{39}Ar$	Mol ^{39}Ar	% Step	Cum. %	$\%^{40}Ar*$	Age [Ma]	±Age
MW-2a (J = 0.006007 ±8.200000e-6)													
1905-01A	1	0	4.61972	0.00485	0.152641	0	4.8507	0.1896	2.9	2.9	9.7	51.81621	2.97838
•1905-01B	0	0	6.96865	–0.00148	0.020829	0	4.19371	0.6095	9.2	12.1	40.5	44.88462	0.54968
•1905-01C	0	0	4.28296	–0.00115	0.006521	0	4.2963	0.9274	14	26	69	45.96875	0.30723
•1905-01D	0	0	3.27547	–0.00098	0.003479	0	4.31316	1.0117	15.3	41.3	80.8	46.14683	0.21683
•1905-01E	0	0	3.67702	–0.00025	0.004171	0	4.34127	0.4678	7.1	48.4	77.9	46.44372	0.38097
•1905-01F	0	0	3.53392	–0.00078	0.003294	0	4.30307	0.659	9.9	58.3	81.6	46.04022	0.29772
1905-01G	0	0	4.96406	–0.00157	0.004202	0	4.13717	0.6567	9.9	68.2	76.9	44.2868	0.29435
1905-01H	0	0	4.92738	0	0.00456	0	4.13685	1.0491	15.8	84.1	75.4	44.28344	0.23377
1905-01I	0	0	4.29457	–0.00108	0.004704	0	4.18339	1.0567	15.9	100	75.1	44.77547	0.25253
Integ. age =												45.3	0.3
(•) Plateau age =									55.5			46	0.3
$^{40}Ar/^{39}Ar$ Step-Heating Data for Run 1905-02; MW-2b													
MW-2b (J = 0.006007 ±8.200000e-6)													
1905-02A	0	0	3.81189	0.00119	0.062124	0	4.47306	0.3743	5.3	5.3	19.6	47.8351	1.37295
1905-02B	0	0	3.11463	–0.00082	0.007532	0	4.40171	1.1188	15.7	21	66.4	47.08201	0.2791
1905-02C	0	0	3.09939	–0.00246	0.004298	0	4.35287	0.9472	13.3	34.2	77.4	46.56624	0.27969
1905-02D	0	0	3.12121	–0.00043	0.003726	0	4.30476	0.9575	13.4	47.7	79.6	46.05808	0.23179
1905-02E	0	0	3.89987	–0.00153	0.003039	0	4.28634	0.7224	10.1	57.8	82.7	45.86353	0.26708
•1905-02F	0	0	4.42672	–0.00095	0.004167	0	4.14442	0.5259	7.4	65.2	77.1	44.3635	0.36646
•1905-02G	0	0	4.62088	0.00045	0.004833	0	4.04798	0.604	8.5	73.7	73.9	43.34342	0.27508
•1905-02H	0	0	4.87148	0.00015	0.005169	0	4.08394	1.1253	15.8	89.5	72.8	43.72388	0.22104
•1905-02I	0	0	4.08489	0.00036	0.006	0	4.1038	0.7501	10.5	100	69.8	43.93394	0.32267
Integ. age =												45.4	0.3
(•) Plateau age =									42.2			43.8	0.3

Step – number of heating steps; Pwr/T°C – degassing power (dot indicate plateau); Ca/K and Cl/K are element ratios; Mol ^{39}Ar – mol ^{39}Ar released at each step; % Step – % of total ^{39}Ar released at each step; Cum. % – cumulative ^{39}Ar release; $\%^{40}Ar*$ – % of ^{40}Ar released; errors are 2-sigma